

Review of Nonlinear Methods and Modelling I

Table of Contents

| | |
|--|----|
| Review of Nonlinear Methods and Modelling I..... | 1 |
| Introduction..... | 2 |
| 1. Basic theoretical concepts..... | 7 |
| 1.1 Dynamic systems..... | 7 |
| 1.1.1 Continuous systems..... | 7 |
| 1.1.2 Discrete systems..... | 8 |
| 1.1.3 Chaos and attractors..... | 10 |
| 1.1.4 Lyapunov exponents..... | 11 |
| 1.1.5 Poincaré sections..... | 13 |
| 1.1.6 Fractal dimensions..... | 13 |
| 1.1.7 Entropies..... | 15 |
| 1.2 Geometry from time series..... | 17 |
| 1.2.1 Embedding..... | 17 |
| 1.2.2 The Grassberger-Procaccia algorithm | 20 |
| 1.2.2.1 Approximate Entropy (ApEn)..... | 22 |
| 1.2.2.2 Sample Entropy (SampEn)..... | 24 |
| 1.2.2.3 Multiscale Entropy (MSE)..... | 24 |
| 1.2.3 Nonlinear prediction and modelling..... | 25 |
| 1.2.4 Noise reduction..... | 27 |
| 1.2.5 Detrended fluctuation analysis (DFA)..... | 30 |
| 1.2.5.1 Disgression: Fourier transform and power laws..... | 33 |
| 1.2.6 Surrogate data..... | 35 |
| 1.2.6.1 Diks' estimator..... | 37 |
| 2. Case studies..... | 40 |
| 2.1 Human balance..... | 40 |
| 2.1.1 Force plate design..... | 40 |
| 2.1.2 COP versus CM..... | 43 |
| 2.1.3 Stiffness hypothesis..... | 45 |
| 2.1.4 Random walk in quiet standing..... | 46 |
| 2.1.5 Disgression: Random walk with relaxation..... | 50 |
| 2.2 Analysis of EMG (ElectroMyoGram) | 51 |
| 2.2.1 Neuromuscular Basics..... | 51 |
| 2.2.2 Modelling EMG..... | 54 |
| 2.2.2.1 Model of IAP..... | 59 |
| 2.2.2.2 The volume conductor model..... | 60 |
| 2.2.2.3 A four-layer model..... | 62 |
| Bibliography..... | 66 |

Introduction

The general objective of time series analysis is to obtain useful information from a signal regarding the state of the *source* of the signal.

Recorded biomedical signals are typically sequences (time series) of readings (measurements) x_n at times t_n , $n = 1, 2, \dots, N$ (the number N of data points is commonly in the range of 10^2 to 10^6). The analysis of such signals is concerned with two main interconnected problems. First we have the task of *denoising* the signal; i.e., to separate (or extract) the relevant biomedical component from the noise, or from the contamination by other “disturbing” biomedical components (e.g. the eye blink from the brain signals in EEG) or the signal conditioning system. Once we have a denoised signal we may have to deal with the second task: *interpreting* the signal, which is, to answer the question: what is the meaning of the signal? One important point to emphasize here (see also [Ruelle, 1994]) is that the effects of the “massage” and filtering by the signal conditioning system may severely complicate the analysis of the data because it is modified by the dynamics of the filter.

In analysing signals we have two basic approaches: the dynamic approach and the statistical approach. The dynamic approaches are outgrowths of the attempts to relate the signals to the bio-physico-mathematical models of the signal source. Statistical methods are typically “ignorant” about the “mechanism” of the source and frame their task as that of finding an optimised *algorithm* (such as the ones based on ARMA-processes [Hänsler, 1997; Moschytz & Hofbauer, 2000]) for predicting new data from old data (e.g. for *control* purposes), or to compute parameters for classification. This algorithm may have no obvious relation to what may be the dynamic details of the source. Thus, the system is regarded more or less as a “black box”. An interesting class of methods is based on *neural networks* [Haykin, 1999] which have especially been used for *classification purposes* and *pattern recognition*, and again, not (primarily) for providing a realistic model of the system at hand.

With the advent of nonlinear times series analysis [Abarbanel, 1995; Diks, 1999; Kantz & Schreiber, 2000; Schreiber, 1998] there has been a convergence between the statistical approaches and the dynamic approaches [Tong 1990, 1995]. Chaotic dynamics has shifted the emphasis from trying to determine the exact path of a dynamic system to calculating *averages* for the paths of the system. Also it has been realised, that the dynamic methods of analysis may be useful even if it cannot be directly ascertained that the system satisfies the criteria for a low dimensional deterministic system. It has been claimed [Rapp et al., 1999; Jones, 2001] that a *new paradigm* has emerged within dynamic system theory - that of *algorithmic modelling*. In algorithmic modelling the starting point is the time series *per se*, not a physico-mathematical model of the system (“newtonian paradigm”). Thus, one uses the time series as the *primary data* and tries to construct an algorithmic model for this data, relevant for the purposes at hand, using methods that have been developed in the theory of dynamic systems. There are at least two theoretical justifications for this approach. First, the nonlinear dynamic theory (originating with the qualitative theory of J H Poincaré (1854 - 1912) has shown that relevant information (useful e.g. for classification purposes, not necessarily for predicting) can be obtained about a dynamic system from a time series generated by this system even if we have limited previous knowledge of the specifics of the system. Secondly, even a very complicated system (such as the heart) may operate in regimes where most of

the *degrees of freedom* are “frozen” and where the system therefore behaves as a low dimensional deterministic system. This point has been forcefully demonstrated by Haken [Haken, 1983, 2000] and his “school” in *synergetics*. Naturally, traditional modelling is still important [Rieke et al., 1999; Keener & Sneyd, 1998; Higgs & Herzog (Eds.), 1995; Koch, 1999; Quarteroni, 2001, 2000; Weiss, 1996; Daune, 1999]. With regard to time series analysis such models can inform us what sort of transitions, patterns, etc., to look for in the signal, and how to effectively extract these features from the time series.

The study of nonlinear dynamic systems has also suggested the existence of so called dynamic *diseases* [Mackey & Glass, 1977; Milton, 2000]; that is, cases where the normal functioning of a physiological system is disrupted, not primarily because of an organic failure, but because the dynamics has been shifted into a critical regime (the reason for this shift could be an improperly working control dynamics). This is compared with how changes of parameters in nonlinear dynamic system may radically alter the behaviour of the system (bifurcation, transition to chaos, etc.). Ventricular fibrillation (VF) and epileptic seizure have been proposed to be instances of dynamic diseases. (In total there are at the present some 30 - 40 types of diseases that have been tentatively identified as belonging to the class of dynamic diseases). A general observation is that healthy organism tend to have chaotic dynamics, whereas disease is related to a more regular state. As e.g. Leon Glass and Joseph Zbilut have pointed out in the context of heart studies that a chaotic dyanmics may be better prepared to swiftly respond to changing conditions.

Thus, chaos, or random fluctuations, may not necessarily be detrimental to the normal functioning of an organism. Indeed, the concept of *stochastic resonance* [Gammaitoni, 1998; Bulsara & Gammaitoni, 1996], originally introduced in physics by R Benzi and coworkers in 1981, has also been found to be of relevance for understanding physiological systems [Moss, 2000]. Stochastic resonance works as an *amplification mechanism* which uses the *random fluctuations* of the environment in order to change the state of the system. A simple example is a particle in a potential well which, without the input of some small amount of random energy, would never be able to get out of it. A biological example would be a subthreshold neural signal which may, with the aid of a random fluctuation, exceed the threshold and thus trigger an action potential – a basic mechanism of amplification which is thought to play an important role in enhancing the sensitivity of biological signal processing systems. The somewhat conterintuitive result is that adding noise to a signal detecting system may enhance its sensitivity - a fact that probably has biological implications.

There is another similar aspect in which chaotic dynamics may enhance the vigilance of living organisms. Thus, instead of an inert stable equilibrium state, a chaotic system may have a *strange attractor* [Ruelle, 1989] such that the system visits continuously all parts of the attractor (this is connected with a so called *ergodic* property). Indeed, this is believed to be an important feature of the brain dynamics. In a sense this property of constantly tracing out its “territory” helps the system to avoid getting trapped into a dead end as suggested above. The “ergodic” property of chaotic system has an interesting consequence from the control theoretical perspective. If one wants to stabilise a certain orbit (or a fixed point) of the system, one has only to wait long enough till the system visits a neighbourhood of the desired orbit and then activate a control mechanism (e.g. by adjusting some of the parameters controlling the dynamics) which will keep the system close to this orbit. This scheme is realised by the so called OGY-control method [Ott, Grebogi & Yorke, 1990]. (The progress towards the desirable control point/orbit can be accelerated by the *method of tracing*.)

The central idea of algorithmic modelling is the construction of a phase space, from time series alone, using the *delay embedding* method [Packard et al., 1980] originally proposed by David Ruelle. A scalar time series x_n , which we suppose is generated by a (bounded) deterministic dynamics, is mapped on vectors

$$z_k = (x_k, x_{k+d}, \dots, x_{k+(m-1)d})$$

where d is the delay, and m the embedding dimension. The vectors z trace out a set in the m -dimensional space R^m . If m is large enough this map will generically unfold the a “diffeomorphic” copy of the original phase space (or rather the subspace where the system dwells). That means that diffeomorphic and topological *invariants* computed for the reconstructed phase space will be the same as the ones we would have computed in the original phase space had it been available to us. Thus, we may get access to characteristics of the original dynamics without any previous knowledge of the system.

A lot of research has been carried out since the 1980’s, when the embedding reconstruction of phase space was first proposed, with regard to the practical applicability of the method as a basis for time series analysis. Generally, good results have been restricted to carefully prepared low dimensional systems (effective dimensions in the range of 2 – 3). In these cases there are reliable and robust methods for calculating *dimensions* (of the attractors), *Lyapunov exponents*, *entropies* and so on, as well as robust and effective algorithms for denoising and (short time) prediction (for algorithms and implementations see [Hegger, Kantz & Schreiber, 1998], and [Kantz & Schreiber, 1997]). In the physiological realm claims of promising results have been reported about applications of the nonlinear time series analysis to the study of brain signals (EEG), especially in predicting the onset of epileptic seizure [Sakellares et al., 1986]. In another application Schreiber and Kaplan [Schreiber & Kaplan, 1996] has successfully employed nonlinear methods for separating mother and foetus ECG-signals. Measures based on nonlinear dynamics (“point correlation dimension” P2Di) are also reported to be able to discriminate, using heart beat data, patients with high risk for ventricular fibrillation (VF) among cardiac patients. The P2Di advocated by Skinner (see [Skinner et al., 1998]) is claimed to work for nonstationary signals. Still, *nonstationarity* is a stumbling block for most time series method used today. Another crucial problem for nonlinear time series analysis are the apparent high dimensional cases [Hegger, Kantz & Olbrich, 1998] - how to distinguish a deterministic high dimensional signal from noise, and how to get reliable measures in high dimensional cases without necessarily an exponential increase in the demand on the size of data?

For classification purposes (diagnosis) the absolute meaning of the parameters are seldom of importance, only the relative orders count. Thus it might be of greater interest to track the *change* of, say, the “dimension“ of a signal rather than its absolute value (which may be difficult to interpret). The fact that sometimes the order of the data, or whether it is above or below a threshold, is more important than the absolute values of the data leads to a great simplification in the form of *symbolic dynamics* [Bai-Lin, 1989]. As an example, one may mark the instant when a time series crosses a threshold by 1, and the other instances by 0, thus replacing the original time series with one consisting only of zeroes and ones. Such a procedure is e.g. justified when one is interested only in the frequency of the changes for instance (typical applications are breathing patterns, heart rate variability, and the study of the synchronisation of signals such as heart rate and breathing). Generally symbolic dynamics is based on *coarse graining*; that is, dividing the phase space into a finite number of cells #1, ..., #n and then recording only in which cell the

dynamic system presides at a given moment. This method naturally effects considerable compactification of the data and also alleviates the sensitivity to noise.

Determinism means that points close to each other in phase space at a time t will probably be close to each other at a time $t + \Delta t$. This property is used in the *Recurrence Quantification Analysis* (RQA) of time series [Eckmann et al., 1987]. Basically one calculates the difference $|z_n - z_m|$ (using the delay embedding) which constitutes the *recurrence matrix* $R_{n,m}$. Deterministic signals will show regular patterns in the recurrence matrix. Besides offering new visual tools (recurrence plots) a number of new parameters can be defined based on RQA – one of the most important ones is the %DET-parameter (“percent determinism”). %DET is about zero for a random signal and close to 100 for a deterministic signal. RQA has been applied to sEMG, heart rate variability, breathing patterns, EEG, etc. One study [Filigoi & Felici, 1999] reports e.g. that “RQA may be proposed as a valid tool for the study of sEMG (...) on of the parameters extracted with the RQA technique, namely %DET, was shown to be a good and reliable measurement of the intrinsic structure of the signal itself”.

In an earlier study [Nieminen & Takala, 1996] applied nonlinear time series analysis to measured (by needle) myoelectric signals (MES) and compared the result with classical ARMA models. The study obtained results that "support the use of the theory of nonlinear dynamics in the modelling of the myoelectric signal". Using nonlinear prediction test [Kennel & Isabelle, 1992] the MES was found to possess "a structure statistically distinguishable from high-dimensional linearly correlated noise". The embedding dimension estimated on the basis of the nonlinear predictability was in the range of 5 to 7. It is also claimed that the dimension (including the "correlation dimension") showed a significant decrease when the muscle fatigued (isometric test). The authors advocate the theory of nonlinear dynamics for "the analysis and modelling of the MES". Of course, already establishing a new significant parameter based on these methods would be an important step, irrespective of whether an explicit model can be devised or not.

Chaotic phenomena, irregular shapes etc., have often been studied by methods from fractal analysis. A recent fractal method is the *detrended fluctuation analysis* (DFA) introduced by Peng et al. [Peng et al., 1994]. It has now become one of the basic methods for analysing heart beat sequences [Peng et al., 2000; Mäkikallio, 1998] and long range correlations in general. The DFA-method divides the integrated time series in blocks of size n for increasing n . For every block one calculates the squared difference between the integrated time series and its best linear fit within the block (this involves the "detrending"). The root square of the sums of these squared differences for block size n defines the "fluctuation" $F[n]$ which is often found to vary as a power of the block size n , $F[n] = n^\alpha$. The exponent α of this power relation defines a pertinent parameter called the *self-similarity parameter* (when applicable it is related to the so-called *Hurst exponent* H by $\alpha = H + 1$). This method can be applied to non stationary series as it is insensitive to slow trends in the data. In one study of brain signals (EEG) [Hwa & Ferree, 2001] they identified two scaling regions in terms of α and speculated that this signifies distinct dynamic processes at work.

A principal motivation behind algorithmic modelling is the fact that we may expect to encounter more and more problems where traditional modelling in terms of explicit functional relations are not available, or too complicated to implement as such. Algorithms therefore become an even more important tool, not just for handling the numerics of traditional newtonian models, but also for the very formulation of the models. The de-

velopment of modern computers and electronic data acquisition systems has also made the use of the algorithmic approach feasible as well as imperative. Yet in the final end the newtonian models are also necessary if we want to understand what is going on. Algorithmic models may work as a bridge between newtonian models and experimental data. In the future we may expect a closer relation between newtonian models, algorithmic models, statistical methods, and time-frequency methods in time series analysis. For instance, we might expect an improved understanding of the molecular dynamics on the cellular level, which in turn may lead to better models for the cell interactions and the signals generated in these processes. Also, in order to be able to design optimal electrodes we need to know how the signals are generated and transmitted through the biological tissue and how they finally interact with the electrode.

1. Basic theoretical concepts

1.1 Dynamic systems

1.1.1 Continuous systems

Generally a continuous dynamic system consists of a manifold M (phase space) and a map (evolution, flow)

$$F: M \times R \times R \rightarrow M$$

such that if the system is in the state $x_0 \in M$ at $t = t_0$ it will have moved to the point $x = F(x_0, t, t_0)$ at time $t \in R$. This is commonly written also as

$$(1) \quad x = F_{t, t_0}(x_0)$$

The Eq (1) epitomises the concept of *determinism*: If the state x of the system is given at a time $t = t_0$ it is determined at any other time t by the map (1). Determinism implies that evolving from time t_0 to t_1 , and then from t_1 to t_2 , is the same as evolving from t_0 to t_2 :

$$(2) \quad F_{t_2, t_0} = F_{t_2, t_1} \circ F_{t_1, t_0}$$

Eq (2) is called the "Chapman-Kolmogorov law". If the evolution in Eq (1) only depends on the *time difference* $t_1 - t_0$ we have a so called *autonomous system* and instead of (1) we may write

$$x(t) = F_t(x_0)$$

which gives the state of the system at any time $t + t_0$ when it was in the state x_0 at (an arbitrary) time t_0 . Eq (2) has for an autonomous system the simple form

$$(3) \quad F_{s+t} = F_s \circ F_t$$

A simple 2-dimensional example is the rotation in the plane $M = R^2$ is given by

$$F_t(x) = \begin{pmatrix} \cos(t) & \sin(t) \\ -\sin(t) & \cos(t) \end{pmatrix} \cdot \begin{pmatrix} x_1 \\ x_2 \end{pmatrix}$$

which rotates the vector

$$x = \begin{pmatrix} x_1 \\ x_2 \end{pmatrix}$$

by t radians clockwise. Typically we do not have an explicit expression for the map F but at best a *differential equation* for the evolution of the system:

$$(4) \quad \frac{dx}{dt} = f(x, t)$$

For autonomous systems the time dependence in the RHS of Eq (4) is dropped. Since the time of Isaac Newton (1642 - 1727) such equations (4) have been the focus of theoretical research in physics (for a modern introduction to Classical Dynamics see e.g. [José & Saletan, 1998]). Only a small ("integrable") subset of the problems in science leading to equations of motion (4) can be solved explicitly. Usually one has to further simplify the equations (by introducing approximations) or/and solve the equations numerically. This is especially true of *nonlinear* problems where the function f in (4) is a nonlinear function in x . A classical one-dimensional simple example of a nonlinear problem which cannot be explicitly solved was given by J Liouville (1809 - 1882) (this is an example of a *Riccati differential equation* - see e.g. [Simmons, 1972], especially problem nr. 8 on p. 248):

$$(5) \quad \frac{dx}{dt} = t - x^2$$

The historically important 3-dimensional example of a dynamic system which was studied by E Lorenz in 1963 [Lorenz, 1963] (as a simplified model of atmospheric dynamics) is given by

$$(6) \quad \begin{aligned} \frac{dx}{dt} &= \sigma \cdot (y - x) \\ \frac{dy}{dt} &= r \cdot x - y - x \cdot z \\ \frac{dz}{dt} &= -b \cdot z + x \cdot y \end{aligned}$$

Because of the nonlinear second order terms on the RHS of Eq (1.1.1-6) the equations can generally only be solved numerically.

1.1.2 Discrete systems

Discrete dynamic systems arise naturally from continuous systems when we try to solve the Eq (1.1.1-4) numerically. This usually implies a discretization of time: $t_n = n \Delta t$,

where Δt is the time step used in numerically integrating Eq (1.1.1-4). The simplest numerical method of integrating Eq (1.1.1-4) is the *Euler method*:

$$(1) \quad \begin{aligned} x_{n+1} &= x_n + f(x_n, t_n) \cdot \Delta t \\ t_{n+1} &= t_n + \Delta t \end{aligned}$$

The smaller the time step Δt the better, in general, will x_n approximate the true value of $x(n\Delta t)$. Whereas the Euler method is sufficient for integrating numerical data (when f is given by empirical data), there are a great number of refinements of the procedure, one of the most frequently used being the *Runge-Kutta method* of 4th order [Abramowitz & Stegun, 1965; Harris & Stocker, 1998], which can be applied when f is a given analytic function.

The general definition of a discrete dynamic system comprises a set M and a map (N is the set of natural integers)

$$(2) \quad F: M \times N \rightarrow M$$

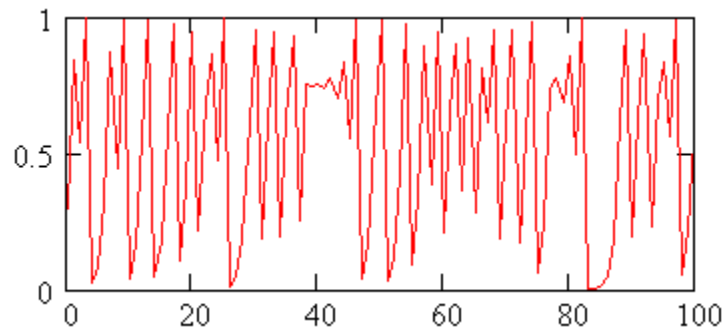
Given a point $x_0 \in M$ we obtain a sequence x_n (an orbit) by

$$(3) \quad x_{n+1} = F(x_n, n)$$

Thus "time" is given as a discrete set of points 0, 1, 2, ... and F describes the evolution for one time step. A much studied discrete nonlinear one-dimensional system is the *logistic map*

$$(4) \quad x_{n+1} = \lambda \cdot x_n \cdot (1 - x_n)$$

For the special parameter value $\lambda = 4$ the map (1.1.2-4) is termed the *Ulam map* (after S Ulam (1909 - 1984)) which exhibits fully developed *chaos*. The figure below shows the time series of the Ulam map with the initial value $x_0 = 0.3$. The time series looks random, yet it is a deterministic series produced by the simple map (1.1.2-4). From Eq (1.1.2-4) we also observe that the evolution is *irreversible*; from x_{n+1} we cannot uniquely determine the previous value x_n .

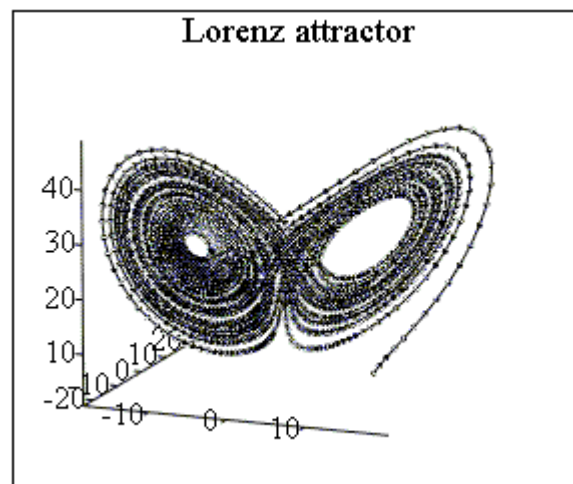


1.1.3 Chaos and attractors

Consider the simple linear one-dimensional system ($\lambda < 0$)

$$(1) \quad \frac{dx}{dt} = \lambda \cdot x$$

which has the solution $x(t) = F_t(x_0) = x_0 \cdot e^{\lambda t}$. Apparently, the set of points $\{F_t(x)\}$ will approach the *equilibrium point* $x = 0$ as $t \rightarrow \infty$ for negative λ . This is an example of an *attractor* which in this case consists of a single point ($x = 0$). In a more general situation the attractor $\{F_t(x): t \rightarrow \infty\}$ may be a submanifold S of the phase space M . Then, for a wide range of initial points x_0 the orbit $F_t(x_0)$ will approach $S \subset M$ as $t \rightarrow \infty$. The figure below shows the attractor of the Lorenz system for the standard parameter values ($\sigma = 10$, $r = 28$, $b = 8/3$).



From the figure it appears as if the attractor would be a complicated 2-dimensional submanifold. Indeed, attractors may be complicated sets, called *fractals*, as they are associated with "fractal dimensions". When studying dynamic systems the attractors may be of intrinsic interest as their structure may give important information about the behaviour of the system. By numerically investigating Eq (1.1.1-6) Lorenz discovered that the evolution of the system had a very sensitive dependence on the initial conditions. Indeed,

two orbits, $x(t)$ and $y(t)$, initially close at a time $t = 0$ tend to diverge at an exponential rate with time ($\lambda > 0$):

$$(2) \quad |x(t) - y(t)| \approx |x(0) - y(0)| \cdot e^{\lambda t}$$

This is a defining property of *chaotic dynamics*. Of course, for a bounded system the difference (2) cannot grow beyond the size of the system. Thus (2) may be approximately valid only for restricted time spans. Anyway, the upshot is that *long range predictions* become virtually impossible. This fact had already been noted theoretically by the mathematician J Hadamard (1865 - 1963) in 1898 in connection with an investigation concerning the geodesics (curves of shortest lengths connecting two points) on manifolds of negative curvature which also lead to diverging paths. For a chaotic dynamics the state x will asymptotically reach an attractor S , but for long time spans it will be impossible to predict *where* on the attractor the point will be. Such chaotic attractors are called *strange attractors*.

The Eq (2) is connected with the concept of *stability*. Suppose $y(0)$ is an *equilibrium point*, and thus $y(t) = y(0)$ remains fixed, then if $\lambda > 0$ Eq (2) means that a small deviation from the equilibrium leads to a growing excursion away from the equilibrium point; thus we have an *unstable* equilibrium. This is a characteristic property of chaotic systems.

1.1.4 Lyapunov exponents

In the limit for small $t > 0$ Eq (1.1.3-2) essentially gives the definition of a *Lyapunov exponent* λ (after A M Lyapunov (1857 - 1918)). Consider two orbits of the system (1.1.1-4) starting at neighbouring points x_0 and $x_0 + \Delta x_0$. The difference (we consider the autonomous case here)

$$\Delta x_1 = F_t(x_0 + \Delta x_0) - F_t(x_0)$$

between the two orbits satisfies the equation (for small Δx_0)

$$(1) \quad \Delta x_1 \approx DF_t(x_0) \cdot \Delta x_0$$

where $DF_t(x)$ is a matrix (the derivative of F_t vis-a-vis x) which determines the "rate of expansion" $e^{\lambda t}$ (cmp. Eq (1.1.3-2)). By computing the average expansion along the orbit $F_t(x_0)$ we obtain the *Lyapunov exponents* λ . If we have a positive Lyapunov exponent for a bounded system, $\lambda > 0$, this indicates that the system is chaotic. Thus, the calculation of Lyapunov exponents is an important method for investigating the properties of a dynamic system. The Lyapunov exponents can be computed by directly measuring the separation of nearby orbits as a function of time and using Eq (1.1.3-2) as a definition of the Lyapunov exponents λ . For a continuous system of dimension n we can define n Lyapunov exponents. Indeed, imagine a small sphere V of radius r at the point $x \in M$. Then the flow F_t of the dynamics will map, for small t , V on an ellipsoid V^* whose main axes, arranged in a descending order, are $r_1 \geq r_2 \geq \dots \geq r_n$. Then the Lyapunov exponents at x can be defined by (in the limit of $t \rightarrow \infty$)

$$(2) \quad \lambda_i = \frac{1}{t} \cdot \log \left(\left| \frac{r_i}{r} \right| \right)$$

Systems with attractors are typically *dissipative systems*; that is, any volume in the phase space will contract during evolution. Given a volume V in the phase space, the flow F_t will map it (for $t > 0$) on a contracted volume. This is equivalent with the sum of the Lyapunov exponents being negative. For bounded continuous systems the Lyapunov exponent in the direction of the flow is *zero* if the trajectory contains no fixed point (deviations along the orbit are mapped on the orbit itself - no separation between two different orbits occurs). Thus, for a chaotic and a dissipative system we must have a dimension $n \geq 3$ since, besides the zero Lyapunov exponent, at least one Lyapunov exponent must be positive (to cause the separation of orbits), and at least one must be negative in order for their total sum to be negative.

From Eq (1.1.1-4) it can be shown that the rate of change of volumes V due to the flow is given by (the "divergence" of f)

$$\frac{\dot{V}}{V} = \nabla \cdot f \equiv \sum \frac{\partial f_i}{\partial x_i}$$

which will be the same as the total sum of the Lyapunov exponents. For the Lorenz system (1.1.1-6) we therefore obtain

$$\lambda_1 + \lambda_2 + \lambda_3 = -\sigma - 1 - b$$

which indeed is negative for the standard choice of parameters ($\sigma = 10$, $r = 28$, $b = 8/3$). Lyapunov exponents are of special interest as they are independent of the co-ordinate system ("diffeomorphic invariant"). This follows because they are obtained by an averaging procedure. The invariance has important implications for the analysis of time series. Indeed, it means that the special representation chosen for the data does not affect the value of the global exponent. Of particular interest is the *maximal Lyapunov exponent* λ_l . A positive maximal Lyapunov exponents signals the presence of chaos. The maximal Lyapunov exponent is obtained as the exponent λ in Eq (1.1.3-2) in the limit of $x(0) \rightarrow y(0)$ and $t \rightarrow \infty$:

$$(3) \quad \lambda_l = \lim_{t \rightarrow \infty} \lim_{\|x(0) - y(0)\| \rightarrow 0} \frac{|x(t) - y(t)|}{|x(0) - y(0)|}$$

The reason why Eq (1.1.4-3) extracts the maximum Lyapunov exponent is because in this limit the factor $e^{\lambda_l t}$ overshadows all the other factors determining the separation of the orbits. The formula in Eq (1.1.4-3) is also quite straightforward to implement numerically.

For discrete systems we can have chaos already in the one-dimensional case as the logistic map testifies. Consider the case of the Ulam map ($\lambda = 4$ in Eq (1.1.2-4)). It has the *fixed point* (or equilibrium) $x^* = 3/4$. Let $w_n = x_n - x^*$ be the deviation from the fixed point, then we have

$$(4) \quad w_{n+1} = -2 \cdot w_n - 4 \cdot w_n^2$$

Thus, x^* is an unstable fixed point of the Ulam map, the deviation growing as the power of 2 with each time step near the fixed point.

1.1.5 Poincaré sections

There is an interesting way (introduced by Poincaré) of obtaining a discrete ($n - 1$)-dimensional dynamics from an n -dimensional continuous dynamics. The case $n = 3$ may illustrate the general situation. Thus, suppose we have an orbit $x(t) = F_t(x)$ in R^3 . A suitably placed (oriented) plane P will intersect the orbit in a discrete set D of points $x(t_k)$ called a *Poincaré section*. We may select those points at which the tangent of the orbit and the normal of the plane point to the same side of the plane (i.e. we may choose the points where the orbit intersect the plane from the "behind"). Since we have deterministic system the point $x(t_k) \in P$ will uniquely determine the point $x(t_{k+1}) \in P$; that is, we have 2-dimensional discrete dynamics (setting $x_k = x(t_k)$)

$$(1) \quad x_{k+1} = G(x_k)$$

in the plane P . The Poincaré section contains the fundamental information about the orbit $x(t)$, such as the Lyapunov exponents (the "redundant" zero-Lyapunov exponent is eliminated in the Poincaré section).

1.1.6 Fractal dimensions

The attractors may have a complicated structure. An important parameter describing geometrical structures is the fractal dimension which generalizes the usual integer valued topological dimension. Mandelbrot [Mandelbrot, 1982] has been the chief progenitor of the field of the fractals. The classical example (L F Richardson, 1963) is the problem of determining the true length of the rugged coast line such as that of England. The shorter the length l of the measuring stick the longer will the measure of the coast line turn out to be. Indeed, using maps of different scales it was empirically found that the total length L varies as a power of the length scale l :

$$(1) \quad L(l) \propto l^{1-D}$$

The parameter D is called the *fractal dimension* of the curve. (For the coast of France it was found that $D \approx 1.204$; for Norway, $D \approx 1.52$; for Portugal, $D \approx 1.115$.) Apparently, for a smooth line $D = 1$, agreeing with the usual topological dimension, because when the length scale l becomes small enough $L(l)$ will no longer depend on l .

Another way to write Eq (1.1.6-1) is as

$$(2) \quad L(l) \propto N(l) \cdot l$$

where $N(l)$ is the minimum number of boxes with side l needed to cover the curve. Comparing (1.1.6-2) and (1.1.6-1) we infer that

$$(3) \quad N(l) \propto l^{-D}$$

This argument can be generalized to other sets than curves. Thus, if for some set $S \subset R^m$, the minimum number of boxes with sides l needed to cover the set scales as (1.1.6-3) in the limit of small l , then the *box-counting dimension*, or the *Kolmogorov capacity*, D is defined as the limit

$$(4) \quad D = \lim_{l \rightarrow 0} \frac{\log N(l)}{\log \left(\frac{1}{l} \right)}$$

This dimension may be difficult to calculate in practice from measurement data. However, one can define [Hentschel & Procaccia, 1983] a sequence of dimensions D_0, D_1, D_2, \dots , among which D_0 is the same as the box-counting dimension D above. Suppose again that $N(l)$ is the minimum number of *disjoint* boxes #1, #2, ..., #n ($n = N(l)$) with side l needed to cover S . Let the number of points of S contained in the box # i be N_i so that probability for a randomly chosen point in S to be in # i is given by

$$p_i = \frac{N_i}{N}$$

Then the *dimension spectrum* is defined by

$$(5) \quad D_q = \lim_{l \rightarrow 0} \frac{1}{q-1} \cdot \frac{\log \sum_{i=1}^{N(l)} p_i^q}{\log(l)}$$

Apparently the definition (1.1.6-5) agrees with (1.1.6-4) in the case $q = 0$. It is possible to take the limit $q \rightarrow 1$ in (1.1.6-5) which results in the *information dimension*

$$(6) \quad D_1 = \lim_{l \rightarrow 0} \frac{\sum_{i=1}^{N(l)} p_i \log p_i}{\log(l)}$$

The name information dimension comes from its close relation to the *Shannon entropy* in the theory of information [Shannon & Weaver, 1949]. The so called *correlation dimension* D_2 is singled out because there are efficient algorithms for its computation [Grass-

berger & Procaccia, 1983]. One can show that D_{q+1}/D_q as a function of the probabilities p_i has a the maximum value 1 whence it follows that

$$(7) \quad D_0 \geq D_1 \geq D_2 \geq \dots$$

Thus, D_2 provides a lower bound for D_1 and D_0 . The name "correlation dimension" for D_2 comes from the terms $p_i \times p_i$ in the sum (1.1.6-5) when $q = 2$ which can be interpreted as the probability for two randomly drawn points from the set S to belong to the same box $\#i$. If points $\{F_n(x): n \rightarrow \infty\}$ are uniformly distributed over the attractor S we have

$$D_0 = D_1 = D_2 = \dots$$

i.e. all the dimensions agree; in the opposite case we have a so called *multifractal*. A difference between the dimensions (1.1.6-5) measures the lumpiness of the distribution of the points in the attractor. Indeed, there is another way to define the sequence of dimensions (1.1.6-5). Let $N_x(r)$ be the number of points of the set $\{F_n(x_0): n \rightarrow \infty\}$ which are inside a circle of radius r around the point $x \in S$. Now one can show that the average of $N_x(r)$ over S , denoted by $\langle N_x(r) \rangle$, scales like r^{D_0} as $r \rightarrow 0$, and that in general

$$(8) \quad \langle (N_x(r))^q \rangle \propto r^{q \cdot D_{q-1}}$$

Power laws are ubiquitous in nature [Mandelbrot, 1982; Schroeder, 1991] and it is therefore also of great interest to investigate the presence of such "laws" in biological systems and time series.

1.1.7 Entropies

The concept of *entropy* stems from thermodynamics (C E G Clausius) and statistical physics (L Boltzmann) and was introduced into the theory of information by C E Shannon (1916 - 2001). In the context of dynamical systems information has to do with the amount of data needed to identify a point (i.e., the length of its "address label", or the number of bits needed to fix the point) in the phase space given a certain minimum size of resolution. If we have a set of points $x_n \in S, n = 1, 1, 2, \dots, N$, and cover S with *disjoint* boxes $\#i$ (with sides l) - defining a *partition* P of S - each box $\#i$ which contains N_i points of the set $\{x_n\}$, then the average *information* in bits needed to identify a point in this set $\{x_n\}$ as belonging to a certain box $\#i$ is given by *Shannon entropy* (where $p_i = N_i/N$ as before)

$$(1) \quad H = - \sum_i p_i \log(p_i)$$

A Rényi (1921 - 1970) defined a sequence of entropies $H_q, q = 0, 1, 2, \dots$ by

$$(2) \quad H_q = \frac{1}{1-q} \cdot \log \sum_i p_i^q$$

If we take the limit $q \rightarrow 1$ we obtain the Shannon entropy (1.1.7-1). Entropies provide also invariant numbers describing the dynamics (and was for this purpose introduced into dynamics by A Kolmogorov), perhaps not as much used as the Lyapunov exponents. Again, it is quite difficult to get reliable estimates of the entropies from experimental data due to the requirement on the size of data; the case $q = 2$ is the most tractable one from the computational point of view. H_2 gives a lower bound for H_0 and H_1 since we have $H_0 \geq H_1 \geq H_2 \dots$. More precisely, for $q > 1$ it can be shown that H_{q+1}/H_q as a function of the probabilities p_i satisfies (similar relation for the dimensions D_q)

$$1 - q^{-2} < \frac{H_{q+1}}{H_q} \leq 1$$

Indeed, the lower bound corresponds to the case $p_i \rightarrow 1$, e.g. for $i = 1$, and otherwise 0. The upper bound corresponds to the uniform distribution $p_1 = \dots = p_n = 1/n$.

If we use a finer and finer partition the sums in (1.1.7-1) and (1.1.7-2) will diverge. However, there is a way of getting a finite limit by *subtracting* entropies. For this, let p_{i_1, \dots, i_m} denote the joint probability, that for an arbitrary n , x_n is in the box $\#i_1$, x_{n+1} in the box $\#i_2$, etc, and define then, generalizing Eq (1.1.7-2)

$$(3) \quad H_q(m) = \frac{1}{1-q} \cdot \log \sum_i p_{i_1, \dots, i_m}^q$$

The *Kolmogorov-Sinai entropies* h_q are then obtained as upper limits of the difference $H_q(m+1) - H_q(m)$

$$(4) \quad h_q = \sup_P \lim_{m \rightarrow \infty} H_q(m+1) - H_q(m)$$

(the supremum limit is over all possible partitions P). The difference $H_q(m+1) - H_q(m)$ gives the increase in information needed to locate a point of the set $\{x_n\}$ in an $(m+1)$ -dimensional space instead of an m -dimensional space. The existence of the limit (1.1.7-4) means that this increment will "saturate" for high values of m . In dynamics the sequence $\{x_n\}$ will correspond to a time series $F_n(x_0)$. The entropy will then be a measure of the rate of the separation of the orbits. Consider a small box B and its transformation $F_t(B)$ by the flow as $t \rightarrow \infty$. The set $F_t(B)$ may become very complicated as time t grows which means that we need more information (number of bits) in order to locate a point of the sequence $\{x_n\}$ in $F_t(B)$ than in B . This increase in the requirement of information for locating a point is reflected in the entropy. Entropy also gives a measure how far in the future it is possible to make predictions for the dynamical system.

1.2 Geometry from time series

1.2.1 Embedding

The arena of dynamics is the phase space. However, measurement data is usually a sequence of real numbers (a time series) x_1, x_2, \dots , and we may have no information about the details of the dynamics. Assuming that the time series is determined by an unknown deterministic dynamics it is still possible, under quite general conditions, to reconstruct its phase space and thus make it possible to apply the theoretical methods for dynamical systems that were described in the previous sections. This is the foundation of *nonlinear time series analysis*. The reconstruction is based on a very simple idea. Typically the differential equation for a dynamical system is equivalent to an m^{th} order differential equation

$$P\left(\frac{d^m x}{dt^m}, \frac{d^{m-1} x}{dt^{m-1}}, \dots, x, t\right) = 0$$

Under quite general conditions there exists a solution $x(t)$ which is uniquely determined by the initial values (at $t = t_0$)

$$\left(\frac{d^{m-1} x(t_0)}{dt^{m-1}}, \frac{d^{m-2} x(t_0)}{dt^{m-2}}, \dots, x(t_0)\right)$$

This means that a phase space for the system may be described in terms of the variables

$$\begin{aligned} y_1 &= x \\ y_2 &= \frac{dx}{dt} \\ &\dots \\ y_m &= \frac{d^{m-1} x}{dt^{m-1}} \end{aligned}$$

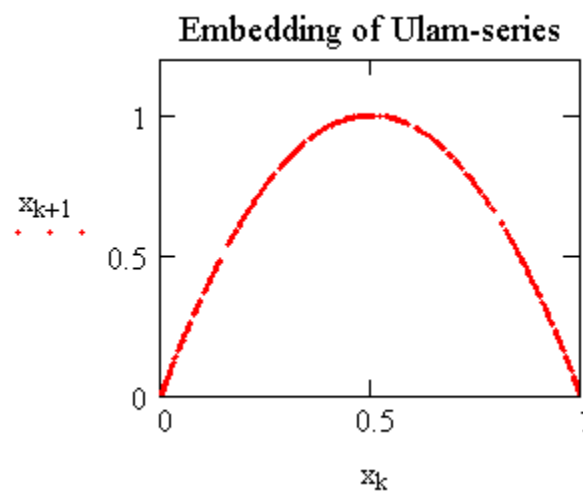
For a discretised system the differential are replaced by differences which means that for the phase space reconstruction we can use as variables (which was suggested by David Ruelle - see [Packard et al., 1980]) the time shifts of x_k :

$$(1) \quad \begin{aligned} y_1 &= x_k \\ y_2 &= x_{k+1} \\ &\dots \\ y_m &= x_{k+m-1} \end{aligned}$$

The form (1.2.1-1) is a special case of a slightly more general form where we use a *delay* d that can be different from 1. Thus, given a (scalar) time series x_1, \dots, x_N , then its m -dimensional embedding in R^m with delay d is given by the vectors

$$(2) \quad \begin{aligned} z_1 &= (x_1, x_{1+d}, \dots, x_{1+(m-1)d}) \\ z_2 &= (x_2, x_{2+d}, \dots, x_{2+(m-1)d}) \\ &\dots \end{aligned}$$

As an example, take the Ulam-time series which is graphed in section 1.1.2. If we map the time series into R^2 using $m = 2$ and $d = 1$ we obtain the figure below.

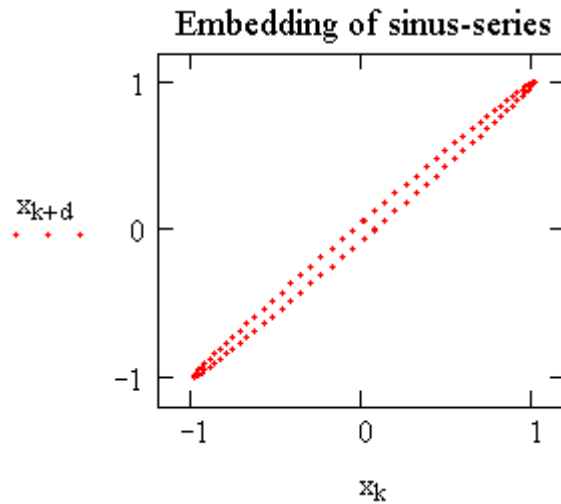


Thus the apparent random series reveals the simple structure of the dynamics when embedded in R^2 . With real data it may not be obvious how to choose the parameters m and d for an optimal embedding. By choosing m large enough the dynamics will indeed unfold, but an excessive large dimension m will be a disadvantage when one wants to extract information from the data about dynamics since typically the requirement on the size of data grows as a power of the dimension m . One method for finding an optimal embedding dimension is to compute the number of *false neighbours* for $m = 1, 2, \dots$. The idea is the following one: Two points which are close in the m -embedding may be so because the time series is a projection of the unfolded trajectory in a higher dimension. Two points not close in the higher dimensional space may get projected close to each other in the lower dimensional space. True neighbours though will remain neighbours when we embed the time series in a higher dimensional space, whereas the false neighbours will get "divorced". Thus, the "optimal" embedding dimension can be chosen as the dimension m beyond which a further increase in the dimension does not resolve any further false neighbours. For a yet another method of determining the embedding dimension see the section 1.2.3 on nonlinear prediction.

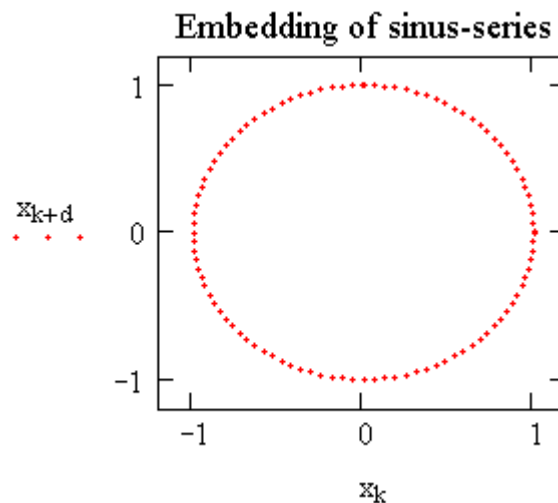
The effect of d can be illustrated by the simple sinus-wave data

$$(3) \quad x_n = \sin\left(2 \cdot \pi \frac{n}{100}\right)$$

If we embed this series using $d = 1$ and $m = 2$ we obtain the graph



i.e., it is almost a diagonal. However, if we use $d = 25$, which is a quarter of the period T ($= 100$) of the wave (1.2.1-3), then we get



which much more clearly shows the trajectory (circle) in the phase space than in the previous case. The point is that if we chose d too small, x_{k+d} will contain almost no new information compared with x_k . If d is too large, on the other hand, x_{k+d} and x_k will be only related like two random numbers (if we have a chaotic dynamics). One idea for determining the delay d is to calculate the *autocorrelation* for the time series,

$$(4) \quad \langle x_n x_{n+k} \rangle = \frac{1}{N} \cdot \sum_{i=1}^N x_i \cdot x_{i+k}$$

(using cyclic convention : $x_{k+N} = x_k$)

and to take d as the value of k where the autocorrelation has reached about $1/e$:th of its maximum value at $k = 0$. Another proposal is to use the *mutual information* $I(k)$, which is a generalization of the autocorrelation, and to take d as the *first point of minimum* of the mutual information (see e.g. [Abarbanel, 1996]). In order to define mutual information for a scalar time series x_n , divide its range into subintervals $\#i$. Then by the histogram method calculate the probability p_i for a point to be in the interval $\#i$, and the joint probability $p_{i,j}(d)$ that if x_k is in $\#i$ (for any k) then x_{k+d} is in $\#j$. Finally the mutual information is defined by the expression

$$(5) \quad I(d) = \sum_{i,j} p_{i,j}(d) \cdot \log \left(\frac{p_{i,j}(d)}{p_i \cdot p_j} \right)$$

Eq (1.2.1-5) describes the amount of information (in bits), averaged over the orbit, "shared" by the signal x_k and its time shift x_{k+d} ; that is, how much we can learn from one signal about the other. Thus, if they are independent we have $p_{i,j}(d) = p_i \cdot p_j$ and the mutual information is zero.

1.2.2 The Grassberger-Procaccia algorithm

Very useful algorithms in nonlinear time series analysis have originated with [Grassberger & Procaccia, 1983]. The basic algorithm consisted in computing the fraction of pairs of points in the embedded space that lie within a distance ϵ of each other. This defines the "correlation" $C(\epsilon)$:

$$(1) \quad C(\epsilon) = \frac{1}{N \cdot (N-1)} \cdot \sum_{i \neq j} \Theta(\epsilon - |z_i - z_j|)$$

where the *Heaviside function* Θ is given by

$$\Theta(x) = \begin{cases} 0 & \text{if } x < 0 \\ 1 & \text{otherwise} \end{cases}$$

From the definition of $C(\epsilon)$ we may expect, if an attractor is present in the system, that its dependence on ϵ reflects the fractal dimension of the the attractor. Indeed, in this case $C(\epsilon)$ will scale as

$$(2) \quad C(\epsilon) \propto \epsilon^{D_2}$$

where D_2 is the correlation dimension discussed earlier. An important improvement to the basic algorithm can be introduced by avoiding pairs of points which are too close in time, because such points tend to lie on a one-dimensional line and thus lead to an underestimation of the dimension in (1.2.2-2). This correction is effected replacing Eq (1.2.2-1) by

$$(3) \quad C(\epsilon) = \frac{2}{(N - n_{\min}) \cdot (N - n_{\min} - 1)} \cdot \sum_{i > j + n_{\min}} \Theta(\epsilon - |z_i - z_j|)$$

where all pairs closer than n_{\min} ("Theiler correction") in time are neglected. (n_{\min} is typically chosen to be around 500, or 10% of the total number of points.)

Corresponding to the series of entropies and dimensions discussed in 1.1.6 and 1.1.7 there is a generalization of (1.2.2-3) which will capture these parameters (for $q > 1$)

$$(4) \quad C_q(\epsilon, m) = \frac{1}{\alpha} \cdot \sum_{i=n_{\min}}^{N-n_{\min}} \left(\sum_{|i-j| > n_{\min}} \Theta(\epsilon - |z_i - z_j|) \right)^{(q-1)}$$

where the normalization factor is given by

$$\alpha = (N - 2 \cdot n_{\min}) \cdot (N - 2 \cdot n_{\min} - 1)^{(q-1)}$$

We have indicated the dependence on m in (1.2.2-4) because $C_q(\epsilon, m)$ is expected to scale as

$$(5) \quad C_q(\epsilon, m) \propto \epsilon^{(q-1) \cdot D_q} \cdot e^{-(q-1) \cdot H_q(m)}$$

As has been pointed out, the case $q = 2$ is generally feasible. The dimensions and entropies are being estimated from (1.2.2-5) by finding *scaling regions* where

$$(6) \quad \log \left(\frac{C_q(\epsilon, m+1)}{C_q(\epsilon, m)} \right)$$

becomes independent of ϵ . The entropy can then be determined if (1.2.2-6) "saturates" with increasing m .

As a "rule of thumb", in order to be able to extract a dimension of value D from the data the minimum size of the should be (D Ruelle)

$$N_{\min} \approx 10^{\frac{D}{2}}$$

Indeed, this follows from Eq (1.2.2-1,2) if we have

$$C(\epsilon_l) \approx N^{-2}$$

at the lower end of the scaling region and

$$C(\epsilon_u) \approx 1$$

at the upper end of the scaling region, and if we require that at least $\epsilon_u/\epsilon_s \approx 10$ for the scaling region in order to be relevant. A somewhat more elaborate heuristic argument in [Hegger et al., 1998] provides the estimate

$$N_{\min} \approx e^{\frac{m \cdot h_2}{2}} \cdot \sqrt{2 k_{\min}} \cdot \left(\frac{\epsilon_u}{\epsilon_l} \right)^{\frac{D_2}{2}}$$

Here k_{\min} is the minimum number of pairs of points needed for acceptable statistics, ϵ_u and ϵ_l are the upper and lower scaling limits of the scaling region in which (1.2.2-5) is numerically valid.

1.2.2.1 Approximate Entropy (ApEn)

An alternative to the steps (1.2.2-1,3) in the case $q = 2$, is the basis for the definition of "approximate entropy" (ApEn) (see e.g. [Yang et al., 2001]) proposed in 1991 [Pincus, 1991] and commonly used in the study of heart beat time series [Mäkikallio et al., 1996]. In the quoted study the neighbourhood size is given in terms of a "tolerance" parameter r (usually chosen to be about 0.2, i.e. 20 %, and with embedding dimension $m = 2$),

$$\epsilon = r \cdot SD$$

where SD is the standard deviation of the time series. In order to compute ApEn one first calculates the quantities

$$C_r^m(i) = \frac{1}{N - m + 1} \cdot \sum_{j=1}^{N - m + 1} \Theta(r \cdot SD - |z_i - z_j|)$$

whose *logarithms* are averaged

$$\phi^m(r) = \frac{1}{N-m+1} \sum_{i=1}^{N-m+1} \ln(C_r^m(i))$$

Finally the approximate entropy is defined as

$$(1) \quad ApEn(m, r, N) = \phi^m(r) - \phi^{m+1}(r)$$

which can be considered as an approximation of the Kolmogorov-Sinai entropy h_2 of Eq (1.1.7-4) (which implies a limit $m \rightarrow \infty$). For large N the expression approximates the logarithm $\ln(1/p)$ of the inverse of the conditional probability p that if two sets of m consecutive points of the time series are close (assuming here a delay $d = 1$); that is,

$$z_k = (x_k, x_{k+1}, \dots, x_{k+m-1})$$

and

$$z_l = (x_l, x_{l+1}, \dots, x_{l+m-1})$$

satisfy $|z_k - z_l| < r \cdot SD$ then we have also $|x_{k+m} - x_{l+m}| < r \cdot SD$. Thus ApEn, like the other entropies, measures a degree of "surprise" in the data, the ability to predict the future behaviour from past patterns. The lower the value of ApEn the more regular and predictable is the data. For instance, in [Yang et al., 2001] they report a study of heart rate tracing from an infant who had an aborted sudden infant death syndrome (SIDS) and one from a healthy infant. The more regular HRV-signal of the SIDS-infant corresponded to a lower ApEn value of 0.826 compared with 1.426 for the healthy infant. The authors emphasise the robustness of ApEn and that it "is not an approximation of the K-S entropy. It is to be considered as a family of statistics and system comparisons (...) with fixed r and m ". The ApEn is said to involve some computational advantages over the traditional K-S entropies: less sensitive to noise, and does not require as many data points for a valid estimate (the typical size of measured biosignals may be only around 1000 points; one rule of thumb [Pincus & Goldberger, 1994] is that a reliable estimate of $ApEn(m, r)$ requires about $10^m - 20^m$ points). Also its ability to differentiate between signals with different mixes of stochastic and deterministic components is emphasized ([Yang et al., 2001], p. 82 - 83).

The study [Mäkikallio et al., 1996] found that ApEn was "significantly higher in a group of postinfarction patients (1.21 ± 0.18) than in a group of healthy subjects (1.05 ± 0.11). In other study [Vikman et al., 1999] a significant decrease in the ApEn was observed before the spontaneous onset of paroxysmal atrial fibrillation (AF).

1.2.2.2 Sample Entropy (SampEn)

One might observe that the "Theiler correction" (see section 1.2.2) is not implemented in the definition of ApEn above so it includes a spurious contribution from "self-matching" because it counts each point z_m as belonging to the neighbourhood of z_m . [Richman & Moorman, 2000] therefore suggested an alternative definition called "Sample Entropy", SampEn. Again, if we have scalar time series x_1, \dots, x_N , consider the m - and $(m+1)$ -dimensional embedding vectors

$$z_k = (x_k, x_{k+1}, \dots, x_{k+m-1})$$

and

$$w_k = (x_k, x_{k+1}, \dots, x_{k+m})$$

and define

$$B_r^m(i) = \frac{1}{N-m+1} \cdot \sum_{j=1, j \neq i}^{N-m} \Theta(r \cdot SD - |z_i - z_j|)$$

$$B_r^m = \frac{1}{N-m} \cdot \sum_{i=1}^{N-m} B_r^m(i)$$

We then define A_r^m exactly the same way using the $(m+1)$ -dimensional vectors w instead of z . Finally the estimate SampEn of the sample entropy (obtained in the limit of $N \rightarrow \infty$) is defined by

$$(1) \quad \text{SampEn}(m, r, N) = -\ln\left(\frac{A_r^m}{B_r^m}\right)$$

Thus, in the limit $N \rightarrow \infty$ it becomes the natural logarithm of the "conditional probability that two sequences within a tolerance r for m points remain within r of each other at the next point". Using numerical simulations [Richman & Moorman, 2000] demonstrates that the SampEn estimate may converge to a consistent value for considerably smaller values of r and N than the approximate entropy estimate. Therefore, the SampEn estimate promises to be less dependent on the data size.

1.2.2.3 Multiscale Entropy (MSE)

The point of departure in [Costa et al., 2002] is the general observation that a "loss of complexity [is] ... a generic feature of pathological dynamics", whereas many entropy algorithms "assign a higher value of entropy to certain pathological time series that are presumed to represent less complex dynamics than to time series derived from healthy function". This circumstance is attributed to the fact that these methods do not take into consideration that the biological processes may have various structures on different time scales. It is therefore suggested that we coarse-grain the data at different time scales and then compute the entropy for every scale and map its dependence on the scale. Thus, given a time series x_1, \dots, x_N , and a scale τ , we define the coarse-grained time series $y^{(\tau)}$ by

$$y_j^{(\tau)} = \frac{1}{\tau} \cdot \sum_{i=(j-1)\tau+1}^{j\tau} x_i$$

$$\left(1 \leq j \leq \frac{N}{\tau} \right)$$

The choice $\tau = 1$ reproduces the original times series. Next [Costa et al., 2002] suggests we calculate the SampEn for the coarse-grained data for a range of scales (in the paper they calculate SampEn for $\tau = 1$ to $\tau = 20$ for data with 30000 points using parameters $m = 2$ and $r = 0.15$). Calculating SampEn as function of the scale is called the multiscale entropy (MSE) analysis. The MSE analysis is expected to reveal whether the data "contains complex structures across multiple time scales". Thus it is found that (correlated) $1/f$ -noise has a higher entropy for scales $\tau > 5$ than (uncorrelated) white noise. Studying heart beat time series it was also found that for $\tau > 6$ the healthy individuals showed higher entropy than subjects with atrial fibrillation (AF) and subjects with congestive heart failure (CHF). At $\tau = 1$ on the other hand the entropy for healthy and CHF coincided at a value much less than the entropy for AF.

1.2.3 Nonlinear prediction and modelling

For deterministic systems the future can in principle be predicted from past data. Deterministic chaos puts limitations on the range of meaningful prediction. Numerical predictions of weather may be of a range of one week. Our planetary system is expected to exhibit chaos on the time scale of some 5 million years (beyond that we cannot give reliable prediction about the whereabouts of the planetary orbits - for a popular review of the topic of the (in)stability of the solar system see [Peterson, 1995]). A general implication of determinism is that points close in phase space are mapped on close points by the flow F_t , for $t > 0$ *sufficiently small*. In terms of an embedded time series, if z_p and z_q are close, then we expect also their time shifts z_{p+1} and z_{q+1} to be close. A simple prediction algorithm is based on this is called the *Lorenz method* - Lorenz did indeed suggest the method. As an (non practical) analogy we may think of weather forecasting. Suppose we have huge record of historical weather data. Knowing the temperature, windiness, cloudiness, etc, of the present day (and for a few days back), we may browse the past record in order to find days (or periods) with similar weather patterns in the past. We then look up how the weather in the past evolved from there on a few days ahead into the future and use that as a prediction for how the weather will be tomorrow etc.

A very simple example ($m = 1$) is the one given by the Ulam-series above. Thus given a number $0 < w_k < 1$ in a similar (unknown) series we may ask what will its next value $w_{k+1} = F(w_k)$ (F is supposed to be unknown). We chose a neighbourhood size ϵ and collect all the terms z_n of a known series within the distance ϵ of w_k . The average of their time shift will then be the prediction for w_{k+1} .

$$(1) \quad w_{k+1}^{\text{pred}} = \frac{1}{\#(S_k)} \cdot \sum_{z_n \in S_k} z_{n+1}$$

$$S_k = \{ z_n : |z_n - w_k| \leq \epsilon \}$$

Of course this procedure can be used for predicting more than one step ahead into the future. Conversely this method of prediction can be used to test the time series themselves in two ways. To begin with we divide the time series in two parts; one used for calculating the predictions, and one part used for checking the predictions so that we can calculate the error of the prediction. Now we can use this setup for determining a minimum embedding dimension m . We compute the error of prediction using $m = 1, 2, \dots$. If m is less than the degrees of freedom (d.f.) of the dynamical system the error will be large. However, when we reach $m \geq \text{d.f.}$ there will be a slump in the size of the error. However, if the error of prediction throughout is no less than if we had made the predictions by "tossing coins" our assumption of a deterministic process is most likely wrong. Thus, the prediction procedure also provides a method for probing whether the time series is deterministic to begin with [Kennel & Isabelle, 1992].

Though the simple prediction algorithm (1.2.3-1) suffices for many purposes, more sophisticated prediction algorithms can be devised by locally approximating the dynamics using e.g. polynomial functions $p_i(z)$, $i = 1, \dots, M$. Given a point y_k in the embedding space, then the idea is that its time shift y_{k+1} can be obtained by a function of the form

$$(2) \quad y_{k+1} = \sum_{i=1}^M c(i, k) p_i(y_k)$$

Thus, Eq (1.2.3-2) constitutes a *model* of the dynamics. The coefficients $c(i, k)$ are calculated using the standard *least square method* (LSM). We form the set S_k of points of the embedded time series in an ϵ -neighbourhood of the point y_k and then we determine the coefficients $c(i, k)$ such that the squared error

$$(3) \quad \sum_{z_i \in S_k} \left(z_{k+1} - \sum_{i=1}^M c(i, k) p_i(z_k) \right)^2$$

is minimized. These coefficients will then be used in Eq (1.2.3-2) for predicting y_{k+1} . They constitute a *local model* of the dynamics around y_k . The next step y_{k+2} is predicted using a local model around y_{k+1} , obtained in the previous step, etc. The root mean square error of this forecast, after L steps, is estimated to grow as [Abarbanel, 1996]

$$(4) \quad N^{-\frac{P+1}{m_L}} \cdot e^{L\lambda_1}$$

N is the number of data, P is the maximum order of the approximation polynomials p_i , λ_1 is the maximum Lyapunov exponent, and m_L is the embedding dimension (it can be less if one employs the so called *principal component analysis* to be discussed below). The second factor in (1.2.3-4) is exactly what we expect from the definition of the Lyapunov exponent.

An interesting application of the prediction algorithms is in the study of a possible *nonstationarity* of a time series. Suppose we divide the time series into subdivisions J_i and then use the data in J_k to predict the data in J_i and thereafter compute the corresponding squared *mutual prediction errors* $e_{k,i}$ (see [Kantz & Schreiber, 1997], § 4.4). If $e_{k,i}$ changes significantly as we move away from the diagonal ($i = k$) this is a sign of a changed dynamics (nonstationarity); that is, the same dynamic rule does not apply to the whole data set.

1.2.4 Noise reduction

Experimental data is always contaminated by noise or other unwanted influences. A classical method of noise separation, filtering, is based on Fourier-spectrum analysis. The simplest version is the use e.g. of a *low pass filter*. It is assumed that the spectrum of the noise (e.g. high frequency vibrations) resides mainly above a certain frequency f_u . The signal is then denoised by dropping all the frequency components with frequency $f > f_u$. In recent decades *wavelet analysis* has become an important tool also in signal analysis complementing the Fourier-analysis. The denoising principles in wavelet analysis are similar to the ones in the Fourier case but one operates on the wavelet coefficients instead of the Fourier-coefficients of the signal. Nonlinear time series analysis provides some novel noise reduction algorithms. The simplest one is based on averaging. Let us explain it in the case $m = 3$ for a time series x_n . Given x_k it will be replaced by an average value calculated as follows: Let S_k be the set of all embedded vectors z_i in an ε -neighbourhood of (x_{k-1}, x_k, x_{k+1}) . Compute the local average

$$(1) \quad \bar{z} = \frac{1}{\#(S_k)} \cdot \sum_{z \in S_k} z$$

and finally replace x_k with \bar{x}_k obtained from $\bar{z} = (\bar{x}_{k-1}, \bar{x}_k, \bar{x}_{k+1})$ in Eq (1.2.4-1). This method corresponds to the averaging of the vector field f determining the dynamics in Eq (1.1.1-4); that is, one averages the flow over a small neighbourhood at every point in the reconstructed phase space. The hope is of course that the random fluctuations will average out. Typically the noise reduction procedure is iterated up to about eight times with decreasing ε . The effect of the noise reduction can be assessed by comparing the predicability of the cleaned data with that of the original data as described in the previous section 1.2.3.

If we think of the attractor as a surface S in R^m , then the effect of noise is typically to spread the points above and below this surface. This suggests that noise reduction can be viewed as a geometrical problem of reconstructing the surface from its bloated version. One solution to this problem is the *local projective denoising method*. It is based on approximating the dynamics locally by linear maps. Geometrically it means that we approximate locally the orbit (attractor) by its tangent space. The noise spreads the point below and above the "true" tangent space. In the projective noise reduction method we try to determine the local tangent space and project the points in the neighbourhood, which have drifted away, back on to the tangent space. Thus, in the cleaned data the points are replaced by their local projections. If m_0 is the smallest integer equal to or larger than the dimension of the attractor, and the data is embedded in a space of dimension $m > m_0$,

then we may suppose that the noise effects a drifting of the points evenly in the $q = m - m_0$ orthonormal directions a^i of the "null space". The projection onto the tangent space is then given by

$$P(z) = z - \sum_{i=1}^q (z \cdot a^i) a^i$$

Again we invoke the least square method in order to determine the orthonormal vectors a^i of the null space. Indeed, we determine a^i such that the squares of the distances of the points in the neighbourhood from the tangent space will be a minimum; this is a generalization of the usual linear regression method of fitting a straight line to set of points and is the content of the *principal component analysis* (PCA). The point of PCA is reduce the dimension of the data space to a subspace where its main variation resides. Now, our problem is reformulated as the minimization of the expression

$$(2) \quad \sum_{i, z \in S_k} (a^i \cdot z)^2 - \sum_i \lambda_i a^i \cdot a^i$$

with respect to the vectors a^i . The last term (2) is due to the constraint that the vectors a^i be of unit magnitude. The minimization of (2) gives the eigenvalue equation

$$(3) \quad C a^i = \lambda_i a^i$$

where the symmetrical positive definite $m \times m$ "covariance matrix" C is defined by

$$(4) \quad C_{rs} = \sum_{z \in S_k} z_r z_s$$

(here z_r denotes the r :th co-ordinate of the point z in R^m). The vectors a^i correspond to the the q eigenvectors of (1.2.4-6) with the *smallest* eigenvalues λ_i . In practice the algorithm is modified by replacing z above in Eqs (2-4) with its deviation from the local average

$$(5) \quad w = R(z - \bar{z})$$

where \bar{z} is the average ("center of mass") of the embedded points in the ϵ -neighbourhood of z_k . R is a *weighing matrix* typically chosen (if $m > 1$) as a diagonal matrix with

the elements (chosen so that $\sum_i \frac{1}{R_{ii}} = 1$, while δ is small number such as 10^{-4})

$$(6) \quad R_{ii} = \begin{cases} \frac{2\delta + m - 2}{\delta} & \text{if } i=1 \text{ or } m \\ 2\delta + m - 2 & \text{otherwise} \end{cases}$$

The point of the weighing matrix is to suppress the contributions by the end co-ordinates of the embedding vectors because they accumulate the greater part of the instabilities. A point x_k of the times series is part of m embedded vectors

$$(7) \quad \begin{aligned} z_k^{(1)} &= (x_k, x_{k+1}, \dots, x_{k+m-1}) \\ &\quad \dots \\ z_k^{(m)} &= (x_{k-m+1}, x_{k+1}, \dots, x_k) \end{aligned}$$

and those of them where x_k is in the middle of the embedding vector will be emphasized using (6) by weighting the correction to x_k from the embedding vectors (7) with $1/R$ (see Eq (9)). The projective correction replaces the embedding vector z_n with

$$(8) \quad z_n^{\text{corr}} = z_n - R^{-1} \sum_{i=1}^q a^i (a^i \cdot R(z_n - \bar{z}))$$

and the correction to x_k is calculated from the weighted mean \bar{z} of the corrected versions of the embedded vectors in (7)

$$(9) \quad \bar{z} = \sum_{i=1}^m \frac{1}{R_{ii}} z_k^{(i)\text{corr}}$$

The nonlinear denoising algorithms described above are of the "blind" type. No knowledge is presupposed about the details of the dynamics. This is typically the case in biological applications. In physical laboratory experiments the situation may be different if one probes accurately modelled systems. Then one can use the explicit model of the dynamics in devising the denoising algorithm (see e.g. [Abarbanel, 1995], ch. 7). Similarly, if one has a clean sample of a signal generated by the source one can use this for a statistical denoising of its contaminated signals.

An interesting and successful application of the nonlinear projective noise reduction method is presented in [Hegger et al., 2000]. They show that the method works on denoising human speech signals though such signals are neither deterministic nor stationary. However, it seems as if the speech signals were approximately deterministic and low dimensional on the phoneme level. In the example cited the authors used embedding dimensions of the order 20 - 30 and a projection to a low dimensional subspace (q in the range of 3 to 7). The neighbourhood size was chosen so as to guarantee 5 to 20 neigh-

bours in the sets S_k above. The large embedding dimensions made the method quite resilient with respect to the noise.

Denoising can be used for *signal separation*. Suppose a signal is superposed by a weaker background signal. Consider first the background signal as "disturbance" and clean it away by denoising the signal. Finally, retrieve the weak signal by subtracting the cleaned signal from the original signal and denoise it. Schreiber and Kaplan [Schreiber & Kaplan, 1996] have used this method together with the projective denoising method for separating mother and foetus ECG. This method works with data from only one channel, whereas e.g. the *independent component analysis* (ICA) [Hyvärinen & Oja, 1999] may require several channels of recordings in order to separate signals by combining inputs from e.g. different locations.

1.2.5 Detrended fluctuation analysis (DFA)

Many signals of biological origin exhibit an absence of characteristic temporal and/or spatial scales (see e.g. [Hastings & Sugihara, 1993; Schroeder, 1991]). Thus it might be that a process $y(t)$ and its time-scaled version $y(at)$ have the same statistics (averages, variances etc.) if we rescale the signal itself too:

$$(1) \quad y(t) \stackrel{d}{=} \frac{1}{a^\alpha} \cdot y(at)$$

The meaning of Eq (1) is that the RHS and LHS have the same statistical properties. A robust method for studying such fractal behaviours of signals was introduced by Peng et alii [Peng et al., 1994] called the *detrended fluctuation analysis* (DFA). The property (1) means that the variance scales as

$$(2) \quad \langle (y(t+\Delta) - y(t))^2 \rangle \propto |\Delta|^{2\alpha}$$

($\langle \rangle$ means averaging over the orbit). Thus, in principle the parameter α can be determined from empirical data by calculating the logarithm of the LHS of (2) for a series of time differences Δ and plot it against the logarithm of Δ . The DFA-method modifies this procedure. First, it is not the signal x itself which is used but its *integration* defined by (for discrete signals)

$$(3) \quad y_k = \sum_{i=1}^k x_i$$

Secondly, suppose the size of the data is N . Then we divide the integrated data y into nonoverlapping blocks of size $n < N$. For every such block we determine its linear least-square fit, which together define a piecewise linear curve yn . Subtracting this from y we get the a "detrended" signal, and the "fluctuation" at level n will be defined by

$$(4) \quad F[n] = \sqrt{\frac{1}{N} \cdot \sum_{i=1}^N (y_i - \bar{y})^2}$$

If y satisfies the scaling property (1,2) then $F[n]$ will follow a "power law"

$$(5) \quad F[n] \propto n^\alpha$$

The exponent α in Eq (5) is termed the *self-similarity parameter*. Generally, a higher α -value implies a more regular time series. It is related to the *Hurst parameter* H defined as α in Eq (2) but *with y replaced by the original signal x* . Since integration raises scaling exponents of the signal by one the Hurst parameter and the self-similarity parameter are related by (when applicable - e.g. for white noise we have $\alpha = 0.5$ but H is restricted to the range $0 < H < 1$)

$$(6) \quad \alpha = H + 1$$

In the range $0.5 < \alpha < 1.0$ we may expect the correlation function to scale as

$$(7) \quad C(\tau) \equiv \langle x(t+\tau)x(t) \rangle \propto \tau^{-\gamma}$$

where $0 < \gamma < 1$ is related to α by

$$(8) \quad \alpha = 1 - \frac{\gamma}{2}$$

Since the Fourier-transformation of the correlation function $C(\tau)$ is equal to the power $S(f)$ the Eq (7) implies that the power scales as

$$(9) \quad S(f) \propto \frac{1}{f^\beta}$$

where β is related to the other parameters by (with certain restrictions on the range of the parameters - for more details see section (1.2.5.1))

$$(10) \quad \beta = 1 - \gamma = 2\alpha - 1 = 2H + 1$$

There is a characteristic difference between signals with $0 < H < 0.5$ and $H > 0.5$. The former is associated with anti-persistence whereas the latter is connected with persistence. Persistence means that for time intervals Δt the values $x(t + \Delta t) - x(t)$ and $x(t) - x(t - \Delta t)$ tend to have the same sign (changes enforce themselves), while in the case of anti-persistence they tend to have opposite signs (changes provoke changes in the opposite direction). More precisely, define ρ -correlation $-1 \leq \rho \leq 1$ for a time scale Δt by

$$(11) \quad \rho = \frac{\langle (x(t+2\Delta t) - x(t+\Delta t)) \cdot (x(t+\Delta t) - x(t)) \rangle}{\sqrt{\langle (x(t+2\Delta t) - x(t+\Delta t))^2 \rangle} \cdot \sqrt{\langle (x(t+\Delta t) - x(t))^2 \rangle}}$$

Now the corresponding *Hurst exponent* H may be defined through (if we have a scaling)

$$(12) \quad \langle (x(t+\Delta t) - x(t))^2 \rangle = \text{const.} \cdot |\Delta t|^{2H}$$

Combining these two relations we obtain

$$(13) \quad \begin{aligned} 2(1 + \rho) &= 2^{2H} \\ (0 < H < 1) \end{aligned}$$

From this we indeed see that the ρ -correlation (11) is negative for $H < 0.5$. Zero ρ -correlation corresponds to the "classical" Brownian random walk. The Hurst exponent can also be directly related to the *fractal dimension* D of the time series as a curve $x(t)$ in the plane by (see e.g. [Hastings & Sugihara, 1993])

$$(14) \quad D = 2 - H$$

Thus the Brown time series $x(t)$ ($H = 0.5$) has the fractal dimension $D = 3/2$. Fractal time series can furthermore be characterised by their *zero-crossing* probabilities. Suppose we have $x(0) = x_0$, then what is the probability that $x(t) > x_0$ for $0 < t < T$ and $x(T) = x_0$? The probability density can be shown [Ding & Yang, 1995] to be related to the fractal dimension D and is inversely proportional to the D th power in T :

$$(15) \quad P(T) \propto T^{-D}$$

a relation that has also been used for numerically determining the fractal dimension D and thus the Hurst exponent for long time series [Liebovitch & Yang, 1997].

Numerous studies have applied DFA to heart beat interval data. In one study it was found (see [Peng et al., 2000]) that for a group of healthy people the self-similarity parameter α was about 1.0 ± 0.1 whereas for a heart failure group it was about 1.24 ± 0.22 .

1.2.5.1 Digression: Fourier transform and power laws

For a signal $x(t)$ of finite duration let us define the correlation by

$$(1) \quad C(\tau) = \int_{-\infty}^{\infty} x(t+\tau)x(t) dt$$

We observe that the correlation function is by definition even, $C(\tau) = C(-\tau)$. Its Fourier transform becomes

$$(2) \quad \hat{C}(f) = \int_{-\infty}^{\infty} e^{-i2\pi f\tau} C(\tau) d\tau = |\hat{x}(f)|^2$$

i.e., the Fourier transform of the correlation function is equal to the power spectrum $S(f)$; conversely, the inverse Fourier transform of the power spectrum $S(f)$ gives the correlation function $C(\tau)$. If we take the inverse Fourier transform of a power spectrum of the variety (1.2.5-9) we arrive at an expression of the form

$$(3) \quad c(\tau) = \int_0^{\infty} \frac{\cos(2\pi f\tau)}{f^{\beta}} df$$

In the case $0 < \beta < 1$ the integral is convergent and by making the variable substitution $f\tau \rightarrow u$ it becomes

$$(4) \quad c(\tau) = \tau^{\beta-1} \int_0^{\infty} \frac{\cos(2\pi u)}{u^{\beta}} du$$

showing that $c(\tau)$ scales as $\tau^{\beta-1}$.

Spectrum power law with $\beta = 1$ is a special case. The corresponding time series is called *pink noise* (or *flicker*), or simply $1/f$ -noise, and has drawn a lot of interest from researchers (see e.g. [Mandelbrot, 1999]). In order to calculate the correlation function for the $1/f$ -noise we will calculate the difference $c(\tau_2) - c(\tau_1)$ in terms of the integral

$$(5) \quad c(\tau) = \int_{\epsilon}^{\infty} \frac{\cos(2\pi f\tau)}{f^{\beta}} df$$

and let ε go to zero. This results in (the last equality is valid for small ε)

$$(6) \quad c(\tau_2) - c(\tau_1) = \int_{\varepsilon\tau_2}^{\varepsilon\tau_1} \frac{\cos(2\pi u)}{u} du \simeq \ln\left(\frac{\tau_1}{\tau_2}\right)$$

Thus, for pink noise the correlation function $C(\tau)$ varies as the logarithm $\ln(1/\tau)$ (plus a "calibration constant" $C(1)$).

The above procedure of introducing a lower cut-off ε for the frequency can also be interpreted in terms of the *renormalization* procedures used in physics. Another approach is based on calculating the Fourier transform of the so-called *principal value* of $1/|f|$ in terms of *distributions* (generalized functions). For a discussion see [Saichev & Woyczyński, 1997, p. 126 – 130]. For $\beta > 1$ Eq (-3) defines a divergent integral and introducing a cut-off produces somewhat arbitrary results in contrast to the $\beta = 1$ case. For β in the range $1 < \beta < 3$ we may instead "renormalize" (-3) by subtracting the infinite constant $c(0)$ from it thus obtaining a convergent integral

$$(7) \quad c_{\text{ren}}(\tau) = \int_0^{\infty} \frac{\cos(2\pi f\tau) - 1}{f^\beta} df$$

Again making the variable substitution $f\tau \rightarrow u$ we get

$$(8) \quad c_{\text{ren}}(\tau) = \tau^{\beta-1} \cdot \int_0^{\infty} \frac{\cos(2\pi u) - 1}{u^\beta} du$$

Thus the "observable correlation" function (for $1 < \beta < 3$) can be expected to be of the form

$$(9) \quad c_{\text{obs}}(\tau) = c_{\text{cal}} - a \cdot \tau^{\beta-1}$$

where c_{cal} is a calibration constant and the parameter a is given by

$$(10) \quad a = \int_0^{\infty} \frac{1 - \cos(2\pi u)}{u^\beta} du = (2\pi)^{\beta-1} \cdot \int_0^{\infty} \frac{1 - \cos(u)}{u^\beta} du$$

Thus if we expect a power spectrum coefficient β to be in the interval $1 < \beta < 3$ it could be estimated from the correlation data by fitting it to a curve of the form (-9) for small time values τ . (Not a very reliable method however.) For power spectrum coefficients β in the range $3 < \beta < 5$ similar methods suggest an observable correlation function of the form

$$(11) \quad c_{\text{obs}}(\tau) = c_0 - c_1 \cdot \tau^2 - c_2 \cdot \tau^{\beta-1}$$

which means that one cannot detect the presence of a power exponent $\beta > 3$ since it is dominated by the second order term for small τ . The Fourier transform of τ^2 in the generalised sense is $-\delta^{(2)}(f)$ (the second derivative of the Dirac delta). The Fourier transform of $|\tau|^{\beta-1}$ for non-integral $\beta > 0$ is given by

$$(12) \quad \frac{2 \Gamma(\beta) \cos\left(\beta \frac{\pi}{2}\right)}{(2\pi f)^\beta}$$

where Γ is the gamma-function defined for $\beta > 0$ by

$$(13) \quad \Gamma(\beta) = \int_0^{\infty} u^{\beta-1} e^{-u} du$$

The result (12) is derived from the expression (13) by allowing complex integration variables in (13).

1.2.6 Surrogate data

"Surrogate data testing attempts to find the least interesting explanation that cannot be ruled out based on the data."

[Schreiber & Schmitz, 1999]

Above we discussed methods for testing for determinism for instance by checking whether there is predicability in time series or not. This may be quite simple for strongly deterministic signals. However, we may have signals that are heavily cluttered with noise and we wish to know if there are residues of deterministic or nonlinear processes that can be traced in the signal. This problem can be formulated as hypothesis testing. The *null*

hypothesis H_0 might be that the signal is generated by a linear gaussian process (*ARMA, Auto Regression and Moving Average*)

$$(1) \quad x_n = a_0 + \sum_{i=1}^{M_{AR}} a_i x_{n-i} + \sum_{j=0}^{M_{MA}} b_j \eta_{n-j}$$

where η_j designate gaussian independent stochastic variables. The coefficients a_i and b_j determine the power spectrum and the correlation function of the generated signal which have to agree with that computed from the measurement data. Using several sets of surrogate data one may compute the values of the *estimator* λ as sequence of nonlinear parameters λ_i , the *estimator* λ may e.g be the correlation dimension D_2 , and compare them with that computed from the measurement data, λ_0 . If λ_0 lies outside, or at the edge of the set λ_i , we might try to estimate the chance that the null hypothesis is false (see e.g. [Kantz & Schreiber, 1997]). One estimator that has been found to be quite reliable is the prediction error (see section 1.2.3). Thus, in a ("non parametric") statistical test where we use the prediction error as the estimator and we choose the probability, that we might reject H_0 though it is in fact true, to be α (typically chosen as 0.05), we have to design a number of $1/\alpha - 1$ sets of surrogate data. If for any of these the prediction error is less than for the original data we *cannot rule out* the null hypothesis given the preset confidence level of $1 - \alpha$. Approximate entropy ApEn discussed in section 1.2.2.1 could also be a candidate for a robust estimator but no systematic investigation seems to have been undertaken regarding this yet.

Demonstrating that the null hypothesis cannot be rejected on the basis of the given evidence does of course not prove that the dynamics is really that of linear gaussian process. The point is rather that the available evidence does not allow us, with the methods at hand, to extract any more subtle structures from the data. For example, few believe that the brain is a linear gaussian process even if the brain waves may have the characteristics of such processes.

A simple method for fabricating surrogate data is the *phase randomization*. For a time series x_n we compute the Fourier coefficients

$$(2) \quad c_k = \frac{1}{N} \sum_{n=1}^N x_n \cdot e^{-i2\pi \frac{k \cdot n}{N}}$$

We then define new coefficients by multiplying the old coefficients c_k with complex unit factors having randomly assigned phases α_k in the interval $(0, 2\pi)$:

$$(3) \quad \bar{c}_k = c_k \cdot e^{i\alpha_k}$$

Applying the inverse transformation to these coefficients we get a series $x^{(s)}_n$.

$$(4) \quad x_n^{(s)} = \sum_{k=1}^N \bar{c}_k \cdot e^{i2\pi \frac{k \cdot n}{N}}$$

This "surrogate data" $x_n^{(s)}$ has the same spectrum and correlation function as the original series x_n , since from (3)

$$(5) \quad |\bar{c}_k| = |c_k|$$

and the correlation function is obtained as the Fourier inverse of the power spectrum. Thus methods based on spectrum and the correlation function cannot distinguish a series and its phase randomised variant. Phase randomised data has been used to test the null hypothesis of linear gaussian process. A more general null hypothesis is obtained if we allow for the possibility that the signal is a static nonlinear transformation $s(x_n)$ of a linear gaussian process x_n . For "nice" forms of the transformation s (i.e. s is invertible and close to identity) we can test this hypothesis by fabricating surrogate data using *Amplitude Adjusted Fourier Transform* (AAFT) (see [Schreiber & Schmitz, 1999]). A very simple procedure is to test for the (somewhat crude) null hypothesis that the data is generated by picking numbers randomly from a set – in this case one creates surrogate data by reshuffling the measurement data in a random way.

Since ARMA processes are time symmetric whereas most nonlinear systems of interest are dissipative one may also use methods for detecting time reversibility as a way to test the null hypothesis of a linear stochastic process. A popular estimator in this case is the 3d order correlation

$$(6) \quad \phi^{\text{rev}}(k) = \frac{\sum_{n=k+1}^N |x_n - x_{n-k}|^3}{\left(\sum_{n=k+1}^N |x_n - x_{n-k}|^2 \right)^{\frac{3}{2}}}$$

1.2.6.1 Diks' estimator

Diks (see [Diks, 1999]) presents a somewhat more advanced method for testing time reversibility which also covers static nonlinear transformations of the linear gaussian processes. The time inversion transformation P is defined by

$$(1) \quad P(x_1, \dots, x_n) = (x_n, \dots, x_1)$$

The time reversibility is then formulated in terms of the map P and the *reconstruction measure* μ . The measure μ is defined in the embedding dimension m by the equivalence (z_n are the embedding vectors in dimension m)

$$(2) \quad \int_{R^m} f(x) d\mu = \frac{1}{N-m+1} \cdot \sum_n f(z_n)$$

for any continuous function $f: R^m \rightarrow R$. Diks then formulates the null hypothesis H_0 of time reversibility as

$$(3) \quad P\mu = \mu$$

($P\mu$ is defined by $P\mu(A) = \mu(P^{-1}A)$ for any set $A \in R^m$.) The idea is then to find an estimator which measures the difference between μ and $P\mu$. For this Diks constructs a metric on the set of measures given by

$$(4) \quad (\mu_1, \mu_2) \equiv \iint K(\mathbf{r} - \mathbf{s}) d\mu_1(\mathbf{r}) d\mu_2(\mathbf{s})$$

where the *kernel* K is chosen to be, for some positive number d (called *bandwidth*),

$$(5) \quad K(\mathbf{x}) = e^{-\frac{|\mathbf{x}|^2}{2 \cdot d}}$$

Now we can define a (squared) difference between μ and $P\mu$ as

$$(6) \quad Q = (\mu - P\mu, \mu - P\mu) = 2(\mu, \mu) - 2(\mu, P\mu)$$

which can be written as

$$(7) \quad Q = \iint g(\mathbf{r}, \mathbf{s}) d\mu(\mathbf{r}) d\mu(\mathbf{s})$$

with

$$(8) \quad g(\mathbf{r}, \mathbf{s}) = 2K(\mathbf{r} - \mathbf{s}) - 2K(\mathbf{r} - P\mathbf{s})$$

This squared difference Q will be the basis for the time reversibility estimator. Indeed, define the w -variables by

$$(9) \quad w_{ij} = g(z_i, z_j)$$

in terms of the embedding vectors z_i . Diks demonstrates that the estimator

$$(10) \quad S = \frac{\hat{Q}}{\sigma(\hat{Q})}$$

under the null hypothesis plus the assumption that the embedding vectors are statistically independent, has a zero mean and unit variance. Here \hat{Q} is the statistical estimate of Q ,

$$(11) \quad \hat{Q} = \frac{1}{\binom{N-T+1}{2}} \sum_{i=1}^{N-T} \sum_{j=i+T}^N w_{ij}$$

(T is the usual Theiler correction discussed in section 1.2.2) and $\sigma(\hat{Q})$ is an estimate of its standard deviation,

$$(12) \quad \sigma(\hat{Q}) = \frac{1}{\binom{N-T+1}{2}} \sqrt{\sum_{i=1}^{N-T} \sum_{j=i+T}^N w_{ij}^2}$$

Indeed, under the given assumptions it can be argued that w_{ij} and w_{kl} ($i \neq j, k \neq l$) are uncorrelated, and that due to time reversibility the values $w_{ij} = \pm a$ have equal probabilities whence \hat{Q} (and therefore \hat{Q}) has zero mean. Typical parameters used by Diks are $m = 3$, $d = 0.2$ and $T \gg m$. One modification (*the block method*) of this procedure in order to reduce the fluctuations of the results is to replace w_{ij} by its average over blocks of the size $l \times l$. An interesting point is that for non reversible series the Diks' estimator S tends to grow with the length of the time series which thus amplifies the discriminatory power of the method. As a rule of thumb, if the null hypothesis is correct then

$$Prob(S > 3) < 0.05.$$

Applying this method to the Wolf sunspot data (using delay = 1, $m = 3$, $d = 0.2$, $T = l = 8$) Diks obtained $S = 5.78$ "which provides strong evidence against the hypothesis that the time series is reversible" ([Diks, 1999] p. 71). A similar analysis of a financial time series (difference of logarithm of IBM stock price, $\log(x_n) - \log(x_{n-1})$) resulted in $S = 1.55$ which does not rule out reversibility (which is expected from the random walk models).

2. Case studies

2.1 Human balance

2.1.1 Force plate design

Standing and walking involve a complex neurophysiological control system. That neurological or muscular disorder may manifest themselves in abnormal patterns in posture and balance is obvious. Making quantitative measurements of the variations in posture remained a technical challenge however. Systematic studies of human stance seems to have begun only with Karl von Vierordt around 1860. Vierordt affixed a feather on the head of his subjects above of which was a sheet covered with lampblack (fine soot). When the subject moved, the feather inscribed a trajectory on the sheet. An electronic force plate was constructed by the French professor Scherrer in 1952. In the 1980's the computer entered the game, used both for data acquisition and analysis. Force was measured with sensors based on pressure gauges or piezo-electric components. The international society of posturography was founded in Amsterdam in 1969 (International Society of Posturography). Posturology seems to be a most active field in countries like France, Italy and Japan. (For historical tidbits and references on posturology see [Gagey & Bizzo, www2001].)

In quiet standing the centre of mass (CM) of the subject makes what seems an erratic bounded trajectory. Suppose the person stands on a rectangular plate supported by force transducers at the corners. The transducers pick up the vertical component of the pressure and we may denote these forces by F_1, \dots, F_4 . Knowing the locations of the transducers we can calculate the centre of pressure (COP). Let the y -axis be in the anterior-posterior direction, and the x -axis along the medial-lateral direction. If sensors are placed at the corners with the co-ordinates $(\pm a, \pm b)$ then the co-ordinates of the COP are given by

$$(1) \quad \begin{aligned} x &= a \cdot \frac{F_2 + F_3 - F_1 - F_4}{F_1 + F_2 + F_3 + F_4} \\ y &= b \cdot \frac{F_1 + F_2 - F_3 - F_4}{F_1 + F_2 + F_3 + F_4} \end{aligned}$$

It can be pointed out here that the subtractions of the forces in (1) help also to cancel external perturbations common to all the transducers. The sum $F_1 + F_2 + F_3 + F_4$ should be almost constant and equal to the weight (W) of the person. The accuracy of the transducers are usually given as percentage p of the nominal load (F_{\max}). Practical measurements seem to indicate that $p F_{\max}$ is the standard deviation of the error of the transducer (the square root of the variance of the fluctuations around the mean value for a constant load). If we assume that errors from the different transducers are statistically independent we can estimate the errors in the COP co-ordinates to be

$$(2) \quad \begin{aligned} \delta x &= 2a \frac{p \cdot F_{\max}}{W} \\ \delta y &= 2b \frac{p \cdot F_{\max}}{W} \end{aligned}$$

For instance, precision force transducers may have $p = 0.02\%$ ($= 0.0002$). Thus, if we use 100 kg sensors ($F_{\max} \approx 1000$ N) and the person has a body mass of 70 kg, and $a = 300$ mm, then we find the error (in the sense of standard deviation) δx to be of the order of 0.17 mm. Using a 16-bit AD-card interfacing the computer the influence of the AD-errors on the total error becomes in this case negligible ($p > 2^{-16}$). The error of 0.17 mm can be compared to typical amplitudes of the sways which are of the order of 10 – 20 mm.



2.1.2 COP versus CM

In static equilibrium the CM and the COP would lie on the same vertical line (i.e. COP would coincide with the projection of the CM onto the x - y plane). This can be illustrated using a simple model, the inverted pendulum [Winter et al., 1998], for the anterior-posterior balance. Here we take the vertical direction as the z -axis. The pendulum rotates around the ankle joint which we take as the orig. in the y - z system. Denote by \mathbf{F} the total force acting on the foot by the force plate at the point $(-\zeta, \eta)$ which is the COP. Finally we denote the CM co-ordinates by (y, z) . From Newton's equations we obtain (L is the distance between CM and the ankle joint, I is the moment of inertia, m is the body mass minus feet mass)

$$(1) \quad \begin{aligned} m \ddot{y} &= F_y \\ m \ddot{z} &= F_z - m g \\ I \ddot{\phi} &= \eta F_z + \zeta F_y - m g L \cos(\phi) \end{aligned}$$

The component F_z is the same force as is obtained from the readings of the force transducers. For small deviations around the z -axis we may replace $\cos(\phi)$ by y/L and as a first approximation we may also set $F_z = mg$, then we obtain from (1)

$$(2) \quad y - \eta \approx \left(\frac{\zeta}{g} + \frac{I}{m g L} \right) \cdot \ddot{y}$$

Thus the difference between the projection of the CM and the COP on the y -axis is proportional to the second derivative of the CM co-ordinate y . We can estimate the difference of $y - \eta$ by approximating the RHS of (2.1-4) as $\frac{L}{g} \cdot \ddot{y}$ and using $L \approx 1$ m. If we assume a sway of 5 mm of the CM in 1 second of time we can estimate \ddot{y} to be around $1/100$ m/s² and the corresponding difference $y - \eta$ to be around 1 mm. If we take the Fourier transform of (2) we obtain the equation

$$(3) \quad \hat{y}(f) = \hat{\eta}(f) \cdot \frac{1}{1 + \frac{f^2}{f_c^2}}$$

where f_c is a characteristic frequency of the body given by

$$(4) \quad f_c = \frac{1}{2\pi} \cdot \sqrt{\frac{g}{\zeta + \frac{I}{mL}}}$$

which can be estimated to be typically around 1/3 Hz for adults. From (3) it is apparent that the CM co-ordinate y is a filtered version of the COP co-ordinate η . This is physically obvious because it takes more energy to move a bigger mass whence vibrations transmitted to a big mass are damped. For slow motions with frequencies f below f_c the co-ordinates y and η trace out almost identical curves, but the high frequency components $f > f_c$ are suppressed in the CM y co-ordinate. If we express (3) in the time domain then the smeared nature of the CM co-ordinate becomes even clearer:

$$(5) \quad y(t) = \pi f_c \cdot \int_{-\infty}^{\infty} e^{-2\pi f_c |t-s|} \eta(s) ds$$

Thus, $y(t)$ is $h(s)$ "averaged" over a time interval whose characteristic size is typically of the order $1/2\pi f_c \sim 0.5$ seconds. Apparently (5) is a *non causal* filter; $y(t)$ will start to change before e.g. we have a spike in η . Indeed, (5) corresponds to a solution of the differential equation (2) for the *boundary conditions* that y vanishes both in the infinite past ($t \rightarrow -\infty$) and the infinite future ($t \rightarrow +\infty$) if η does. Also (5) leaves constant signals unchanged. If we treat (2) as an initial value problem we get for the solution

$$(6) \quad y(t) = 2\pi f_c \int_0^t \sinh(2\pi f_s(s-t)) \eta(s) ds + y(0) \cdot \cosh(2\pi f_s t) + \frac{\dot{y}(0)}{2\pi f_s} \cdot \sinh(2\pi f_s t)$$

2.1.3 Stiffness hypothesis

An complementary analysis can be formulated in terms of "stiffness" [Winter et al., 1998]. Suppose a deviation by an angle α from the vertical is opposed by muscular torque $K \cdot \alpha$ around the ankle joint, with K as the "spring constant". This torque must be equal to $\eta F_z + \zeta F_y$ in (2.1.2-1) otherwise there would be a nonzero total torque acting on the foot making it rotate. With $\alpha = \pi/2 - \phi \approx y/L$ we thus obtain

$$(1) \quad K \frac{y}{L} \approx \eta m g + \zeta m \ddot{y}$$

The last term on the RHS of (1) may be of the order 10^{-4} times smaller than first one whence y is quite nearly proportional to η and thus in phase with it. In terms of the angle α we further obtain the equation

$$(2) \quad \ddot{\alpha} + \left(\frac{K - m g L}{I} \right) \cdot \alpha = 0$$

which implies a natural frequency of

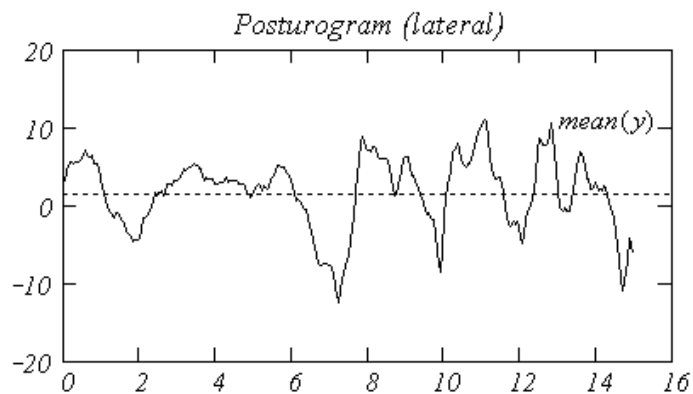
$$(3) \quad f_n = \frac{1}{2\pi} \sqrt{\frac{K - m g L}{I}}$$

Accordingly, if the maximum velocity of sway is v_0 we can predict the amplitude y_0 of the sway to be

$$(4) \quad y_0 = \frac{v_0}{2\pi f_n}$$

Conversely, knowing y_0 and v_0 from measurements we can estimate f_n and the "stiffness constant" K . In the cited study they were able to independently measure the COM coordinate y using markers and optical trackers. Then by determining the angle $\alpha \approx y/L$ and the restoring torque $M = mg\eta$ they were able to establish a relation (linear regression typically with $R^2 = 0.954$) between α and M and calculate the stiffness constant from $K = dM/d\alpha$. Average values obtained by [Winter et al., 2001] for the stiffness (anterior/posterior) was about 430 N m/rad per ankle joint.

Without the K -term the Eq (2) of course describes an unstable situation (the inverted pendulum topples over). Adding the stiffness term $K > mgL$ is the simplest way of stabilising the system (a frictional term would also be needed in order for the system to settle down in the position $\alpha = 0$). Very likely there is a corresponding mechanism in the nature, at least as a linear approximation of a more complicated restoration force. The stiffness model does however not explain the random walk characteristics [Collins & De Luca, 1994] of quiet standing. The figure below shows the sways in medial-lateral direction in terms of COP (in mm along the y -axis in the graph) in a 15 seconds trial. The dotted line is the average position $mean(y)$.



2.1.4 Random walk in quiet standing

That there is a random component in the swaying during quiet standing seems to be well established [Collins & De Luca, 1994; Duarte & Zatsiorsky, 2000], but to what extent this randomness is due to deterministic chaos or some stochastic influence is not settled. Viewing the posturogram as a fractal curve and calculating its Hurst exponent there seems to be a critical value for the size of time interval Δt around 1 sec (cmp Eq (1.2.5-12)) such that the Hurst exponent calculated for $\Delta t < 1$ sec tend to be larger than 0.5 while for time intervals $\Delta t > 1$ sec it tend to be smaller than 0.5. (The analysis of posturograms in terms of random walk and fractal properties is called *stabilogram diffusion analysis*, SDF, in the litterature.) This would mean that we have persistence for small time intervals and antipersistence for large time intervals. Indeed, for short time intervals we might suppose that the inertia will tend to keep the body moving in one direction. On the other hand the motion is bounded (otherwise the person topples over) whence for longer time intervals there will be a reflection of the motion in the opposite direction. Thus, qualitatively the inertia and the boundedness seem to imply the persistence and antipersistence regimes of the swaying. It is simple to enlarge the Eq

(2.1.3-2) with a stochastic term so as to get the random walk signature of the swaying. A somewhat more detailed model (still based on the inverted pendulum) has been presented by [Peterka, 2000] in terms of PID-control systems known from engineering (see e.g. [Khoo, 2000] for a physiological context of these methods). Basically it's an ARMA-process. We present the model here in the familiar form of a differential equation (we have dropped a time delay used in the original formulation since it does not seem to affect the results for this model):

$$(1) \quad I \ddot{\alpha} + K_D \dot{\alpha} + (K_P - mgL) \cdot \alpha + K_I \int_0^t \alpha(u) du = \frac{1000}{\tau_f} \cdot \int_0^t e^{-\frac{(t-u)}{\tau_f}} n(u) du$$

The K -parameters represent the standard PID-parameters: the damping parameter K_D , the stiffness parameter K_P and the integral parameter K_I (which controls the steady-state deviation from the upright position, $\alpha = 0$). On the right hand side we have Gaussian white noise $n(t)$ (uncorrelated) with unit variance and zero mean. The factor of 1000 on the RHS determines the amplitude of the sways, whereas the integration on the RHS acts as a lowpass filter with a characteristic frequency $1/\tau_f$. We quote typical parameter values used by [Peterka, 2000] and expressed in MKS-units.

| Parameter | Value (MKS) | Explanation |
|------------------|--------------------|---|
| I | 66 | moment of inertia vis-à-vis ankle joints (kg m ²) |
| m | 76 | body mass exclusive feet (kg) |
| K_D | 257,8 | damping parameter (N m s rad ⁻¹) |
| K_P | 1117 | stiffness parameter (N m rad ⁻¹) |
| K_I | 14,3 | integral parameter (N m s ⁻¹ rad ⁻¹) |
| L | 0,86 | distance from ankle joints to CM (m) |
| τ_f | 80 | lowpass filter time scale (s) |

The Eq (1) can be conveniently handled numerically if we take the Fourier transform. Thus, one generates the Gaussian noise, takes its Fourier transform, applies the lowpass filtering obtaining $\hat{n}_{\text{filt}}(\omega)$, expresses the Fourier transform of the angle $\hat{\alpha}(\omega)$ in terms of the $\hat{n}_{\text{filt}}(\omega)$, and finally applies the inverse Fourier transform obtaining the angle $\alpha(t)$. Indeed, Eq (1) in the frequency domain is:

$$(2) \quad \hat{\alpha}(\omega) = \frac{1}{K(\omega)} \cdot \frac{1000}{1 + i\omega\tau_f} \cdot \hat{n}(\omega)$$

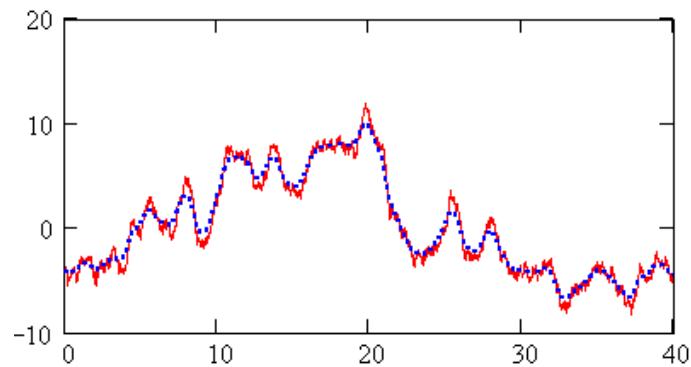
where

$$(3) \quad K(\omega) = -I \cdot \omega^2 + K_D i \omega + K_p - m g L + K_I \cdot \frac{1}{i \omega}$$

The CM-sway in mm will be given by

$$y = 1000 \cdot L \cdot \alpha$$

Using Eq (2.1.2-3) we obtain the Fourier transform of the COP co-ordinate η from that of α . The figure below shows a simulated example of COP trajectory $\eta(t)$ (solid line) and CM trajectory $y(t)$ (dotted line) in millimeters along the vertical axis and with time (seconds) along the horizontal axis. This result was obtained by the Fourier transform method described above using the time step $\Delta t = 0.01$ s. (An artefact of the Fourier method is that the trajectory always ends and starts at the same value due to the periodicity of the sinus and cosinus functions in the Fourier expansion. For unbiased statistics one may use only parts of the simulated curve.)



From (2) we may directly obtain the spectrum $|\hat{y}(\omega)|^2$ for the CM co-ordinate y . With the above choice of parameters there is evidence for a "critical point" around the natural frequency

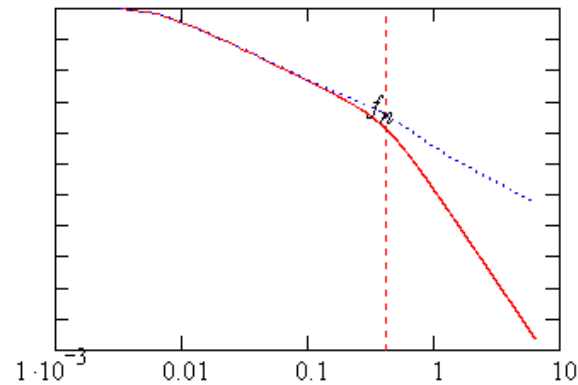
$$(4) \quad f_n = \frac{1}{2\pi} \sqrt{\frac{K_p - mgL}{I}} \approx 0.42 \text{ Hz}$$

where the power curve changes its slope (in a log-log graph). In the figure (log-log plot) below the solid line describes the theoretical spectrum for the CM trajectory while the dotted line describes the spectrum of the COP trajectory obtained from

$$(5) \quad |\hat{\eta}(\omega)|^2 = \left(1 + \frac{\omega^2}{\omega_c^2}\right)^2 \cdot |\hat{y}(\omega)|^2$$

where

$$(6) \quad \omega_c = 2\pi f_c = \sqrt{\frac{mgL}{I}}$$



There is much less dramatic change in the spectrum of the COP co-ordinate. Still if we compute the slope $-\beta$ of its spectrum (in the log-log graph) for the section $f < f_n$ (β_l , for long time) and the section $f > f_n$ (β_s , for short time) we obtain in this example

$$\beta_l \approx 1.685$$

$$\beta_s \approx 2.249$$

with the corresponding Hurst exponents (see Eq (1.2.5-10))

$$H_l \approx 0.343$$

$$H_s \approx 0.624$$

Thus, the model seems to be able to describe the observed persistence for short time intervals ($H_s > 0.5$) and the antipersistence for long time intervals ($H_l < 0.5$). Whether such a PID-control scheme is realised in nature is an open issue. The nervous system may rely on inputs from e.g. muscle spindles, joint receptors, vestibular sensors in the inner ear (semicircular canals, otolithic organs), gravity receptors in the trunk, plus visual cues. Also it has to be pointed out that the inverted pendulum model is only a first approximation. Especially elder people tend to control the stance using the so-called "hip strategy"; i.e., shifting the position of the CM by bending the body.

2.1.5 Disgression: Random walk with relaxation

Apparent different "scaling regimes" may seem to result when one combines random walk with a friction term as in the following simple model (see e.g. [Hastings & Sugihara, 1993]) which is a Langevin-equation on differential form:

$$(1) \quad dx(t) = -r x(t) dt + dB(t)$$

Here the increment dB represents uncorrelated noise with zero mean. The formal solution with $x(0) = 0$ can be written as

$$(2) \quad x(t) = \int_0^t e^{r(s-t)} dB(s)$$

We have especially

$$(3) \quad \begin{aligned} x(t+\Delta t) &= e^{-r\Delta t} x(t) + \Delta W(t) \\ \Delta W(t) &= e^{-r\Delta t} \int_t^{t+\Delta t} e^{r(s-t)} dB(s) \end{aligned}$$

with $\langle \Delta W(t) \rangle = 0$ and $\langle \Delta W(t) x(t) \rangle = 0$ by assumption. For a long time t enough the process becomes stationary since from

$$(4) \quad \langle x(t+\Delta t)^2 \rangle = e^{-2r\Delta t} \langle x(t)^2 \rangle + \langle \Delta W \rangle^2$$

we obtain

$$(5) \quad \langle x(t+n\Delta t)^2 \rangle = e^{-2rn\Delta t} \langle x(t)^2 \rangle + \langle \Delta W \rangle^2 \frac{1 - e^{-2rn\Delta t}}{1 - e^{-2r\Delta t}}$$

which approaches (introducing a parameter σ)

$$(6) \quad \frac{\langle \Delta W \rangle^2}{1 - e^{-2r\Delta t}} \equiv \sigma^2$$

as n goes to infinity.

Thus for large times t we may set

$$(7) \quad \langle x(t)^2 \rangle = \sigma^2$$

Using Eqs (7) and (3) we can finally show that

$$(8) \quad \langle (x(t+\Delta t) - x(t))^2 \rangle = 2\sigma^2 \cdot (1 - e^{-r\Delta t})$$

Compare this with the definition of the Hurst exponent H in Eq (1.2.5-12). Apparently, for $\Delta t \ll 1/r$ we have $H \sim 0.5$; for $\Delta t \sim 1/r$ one might obtain a value $0 < H < 0.5$, and finally for $\Delta t \gg 1/r$ the Hurst exponent H would be concluded to be close to zero. Thus we may expect different "scaling regimes" if one calculates the Hurst exponent from the data without regard to whether there is a real scaling or not. In this model there is a true scaling regime only for short time intervals. We can also look at the situation from the frequency point of view. Eq (3) implies that the correlation $C(\tau)$ is proportional to $\exp(-r|\tau|)$ whose Fourier transform is

$$(9) \quad \int_{-\infty}^{\infty} e^{-i2\pi f\tau} e^{-r|\tau|} d\tau = \frac{2r}{r^2 + 4\pi^2 f^2}$$

Thus, for small frequencies f (long times) the spectrum is almost constant ($\beta = 0$ in which case the Hurst exponent is undefined), whereas for large frequencies (short times) the power spectrum approaches $1/f^2$. If we calculate the correlation ρ defined by Eq (1.2.5-11) we obtain

$$\rho = -\frac{1}{2} \cdot (1 - e^{-r\Delta t})$$

which implies anti-persistence for all time scales Δt .

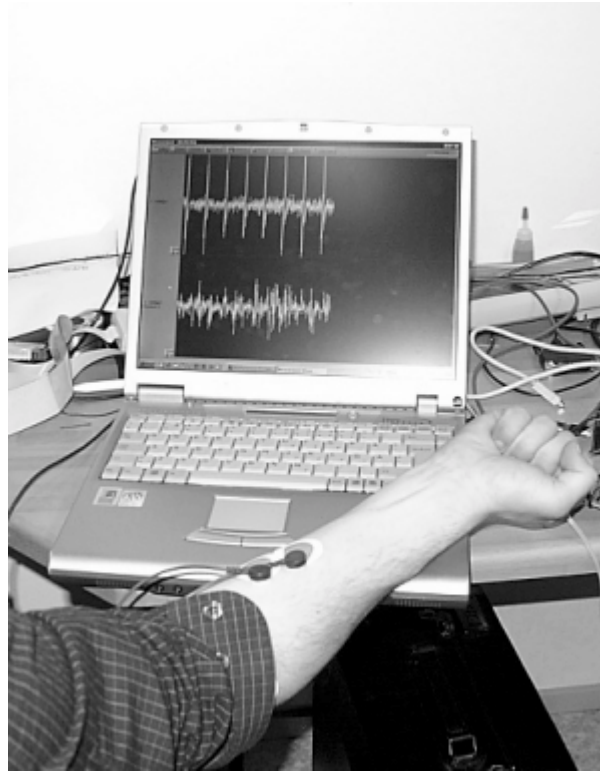
2.2 Analysis of EMG (ElectroMyoGram)

2.2.1 Neuromuscular Basics

That there is connection between electricity and muscle activity was discovered by Luigi Galvani already in 1781. Jan Swammerdam had made similar experiments more than a century earlier (1664) but it is unclear whether he was aware of the role of the electricity in his experiments. A more detailed study of the phenomenon had to wait for developments in anatomy, microscopy and electronics (for historical tidbits see e.g. the introductory chapter in [Malmivuo & Plonsey, 1995]). Skeletal muscles are composed of muscle fibres controlled by the somatomotor nervous system. The muscles exert force

when the fibres are contracting. The contraction is effected by the action potentials (AP), descended from an alpha-motoneuron, which generate muscle fibre action potentials, MAP, which travels in both directions from the motor end plate along the fibres. The action potential along the motoneuron dendrites travels much faster, around 60 m/s, than the muscle action potential along the fibre which may travel with a velocity around 4 m/s. An alpha-motoneuron may control anything from only a few muscle fibres to thousands of muscle fibres (when only gross control of the movements is needed). The alpha-motoneuron, its junctions and the muscle fibres it innervates, are collectively called a *motor unit*, MU. Motoneurons that end up on the same muscle constitute a *motor pool*. If electrodes are inserted into the muscle they may record a sum of the fibre action potentials, whose waveform is called the *motor unit action potential*, MUAP. For a sustained contraction the alpha-motoneuron has to emit a train of action potentials, causing a similar train of motor unit action potentials, MUAPT. The intensity of the contractions is determined by the *firing rate* of the alpha-motoneuron. A few random elements are involved in the neuromotoric process. For example, the release of the acetylcholine (ACh) packets at the neuromuscular junctions is a random discharge causing a random excitation of the muscle fibres called *jitter*. Generally the fibers in a motor unit are activated simultaneously (save for the shifting delays due to varying lengths of the dendritic connections from the motoneuron), but sometimes some of the fibers fail to fire which also adds to the randomness of the total potential.

For surface muscles it is possible to detect a gross electrical activity (the recorded signal is called a *surface electromyogram*, sEMG) of the muscles using surface electrodes. This technique was pioneered by H Piper back in 1912. The amplitude of the muscular action potential is of the order from a few μV to 1000 μV . The frequency content of the MAP is in the range from a few Hz to 10 kHz, but due to filtering by skin, fat, etc., the sEMG is believed to contain relevant information only up to about 500 Hz. The part below 20 Hz is usually filtered out because it may contain motion artefacts and traces from the electrocardiac potentials. surface EMG usually records the superposition of MAPs from many motor units and may also contain crosstalk from other muscles. Using arrays of electrodes it may be possible to isolate individual motor unit components. For a standard reference on electromyography consult [Basmajian & de Luca, 1985]. Recent reviews, together with many references, on the advances in EMG modelling and analysis can be found in the special issues of *Medical Engineering and Physics* (Vol. 22, issues 6 - 7, 1999) and *Journal of Electromyography and Kinesiology* (Vol. 10, 2000).



The most common parameters used in the study of EMG is the *integrated rectified EMG* (iEMG), the *Random Mean Square value* (RMS), the *average frequency* and the *median frequency*. The two first parameters are defined for a given period T and EMG-signal m as:

$$iEMG(t) = \int_t^{t+T} |m(s)| ds$$

(1)

$$RMS(t) = \sqrt{\frac{1}{T} \cdot \int_t^{t+T} |m(s)|^2 ds}$$

The average frequency f_{av} is defined with respect to the spectrum of the EMG-signal as

$$(2) \quad f_{av} = \frac{\int f |\hat{m}(f)|^2 df}{\int |\hat{m}(f)|^2 df}$$

The median frequency f_m is defined such that

$$(3) \quad \int_0^{f_m} f |\hat{m}(f)|^2 df = \frac{1}{2} \cdot \int f |\hat{m}(f)|^2 df$$

One can also trace the time evolution of the frequency parameters by dividing the EMG times series into subintervals and calculate the spectrum for each subinterval and then use Eqs (2 - 3).

2.2.2 Modelling EMG

A MAP travelling along a fibre with a velocity v (taken to be aligned with the x -axis) may be described by a "wave-function"

$$(1) \quad g(x - vt)$$

which describes the voltage amplitude of a travelling wave at the time t and the point x . Thus, the signal $h(t)$, recorded at a fixed point x_0 , as a function of time t is given by

$$(2) \quad h(t) = g(x_0 - vt)$$

If we have a train of MAPs arriving at times t_1, t_2, \dots, t_n we can write the signal at x_0 as a sum of pulses (MUAPT)

$$(3) \quad u(t) = \sum_{i=1}^n h(t - t_i)$$

It is generally believed that the interpulse intervals (IPI) $\tau_i = t_i - t_{i-1}$ are generated by a stochastic process. The average number of pulses λ per time is termed the *firing rate*. If we take the Fourier transform of (3) we obtain

$$(4) \quad \hat{u}(f) = \sum_{k=1}^n e^{-i2\pi f t_k} \cdot \hat{h}(f)$$

If we further take the absolute square of (4) we get for the power spectrum

$$(5) \quad |\hat{u}(f)|^2 = |\hat{T}(f)|^2 \cdot |\hat{h}(f)|^2$$

with the transfer function power spectrum given by

$$(6) \quad |T(f)|^2 = n + 2 \sum_{j>k} \cos(2\pi f(t_j - t_k))$$

If the interpulse intervals τ_k are independent random variables with probability density function (pdf) $p(\tau)$ then the *statistical average* of the transfer function power spectrum can be expressed as

$$(7) \quad n + 2 \sum_{k=1}^{n-1} (n-k) \cos(k\alpha) |\hat{p}(f)|^k$$

where $\hat{p}(f) = |\hat{p}(f)| e^{i\alpha}$ is the Fourier transform of the probability density. In the limit of $n \rightarrow \infty$ Eq (7) can be simplified by carrying out the summation (reduced to a simple geometric sum) and taking the average over the number of pulses n :

$$(7^*) \quad \frac{|\hat{T}(f)|^2}{n} = \frac{1 - |\hat{p}(f)|^2}{|1 - \hat{p}(f)|^2} = \frac{1 - |\hat{p}(f)|^2}{1 - 2|\hat{p}(f)| \cos(\alpha) + |\hat{p}(f)|^2}$$

(this essentially the same expression as that given by [Basmaijan & de Luca, 1985, p. 75]). We consider an example where the interpulse intervals are approximated by a Gaussian pdf

$$(8) \quad p(\tau) = \frac{1}{\sqrt{2\pi}\sigma_\tau} e^{-\frac{(\tau - \tau_m)^2}{2\sigma_\tau^2}}$$

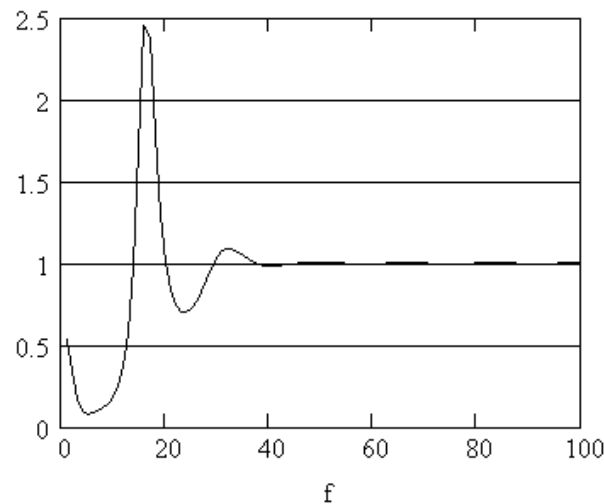
Its Fourier transform becomes

$$(9) \quad \hat{p}(f) = e^{-i2\pi f \tau_m} e^{-2\pi^2 f^2 \sigma_\tau^2}$$

Computing the average over the n pulses we obtain in this case from (7) the factor

$$(10) \quad 1 + 2 \sum_{k=1}^{n-1} \left(1 - \frac{k}{n}\right) \cos(2\pi f k \tau_m) e^{-k 2\pi^2 f^2 \sigma_\tau^2}$$

which apparently acts as a high-pass filter modulated with a frequency $1/\tau_m$. An example of some physiologically realistic values could be $\tau_m = 60$ ms and $\sigma_\tau = 12$ ms. Eq (10) is in qualitative agreement with interpulse interval data (see [Basmaijan & de Luca, 1985, p. 78]) and reaches a practically flat spectrum for $f > 2/\tau_m$ (≈ 33 Hz in the present example).



The size of the first peak is sensitive to the size of the standard deviation σ_τ . Indeed, suppose the interpulse intervals are constant ($\sigma_\tau \rightarrow 0$), $\tau_i = \tau_m$ ($i = 1, 2, \dots$), then (10) will approach a sum of peaks at the points k/τ_m . This follows from Poisson's summation formula (see e.g. [Saichev & Woyczyński, 1997, p. 271]) which in this context reads

$$(11) \quad \sum_k e^{-ik2\pi f\tau} = \sum_k \delta(f\tau - k)$$

where $\delta(x)$ is the Dirac delta function. On the other extreme side (uniform distribution), if $\sigma_\tau \rightarrow \infty$ then (10) approaches the constant function 1.

In sEMG the electrodes will detect MUAPT from several muscle fibers and we have therefore to consider a sum of MUAPTs (3)

$$(12) \quad m(t) = \sum_{p=1}^N u^{(p)}(t)$$

Also the parameters characterising the interpulse intervals may change with time due e.g. to fatigue. A general observation is that the conduction velocity v of the fibres decreases with fatigue. The decrease in the conduction velocity is thought to be linked to the decreasing pH-value in the fatiguing muscle. From Eq (3) we obtain that

$$(13) \quad |\hat{h}(f)| = \frac{1}{v} \left| \hat{g}\left(\frac{f}{v}\right) \right|$$

which suggests that the power spectrum is shifted toward the lower end when the velocity v decreases. It is indeed observed that during fatigue (at constant force level) the *median* and the *average frequencies* of the power spectrum tend to *decrease*. Indeed, if we compute the *average* frequency of the spectrum (ignoring $T(f)$ for the moment) we obtain

$$(14) \quad \frac{\int f |\hat{h}(f)|^2 df}{\int |\hat{h}(f)|^2 df} \propto v$$

according to (13), which predicts a decrease of the average frequency due to decreasing velocity v . This is because the "energy" (the denominator in (14)), the integrated power, is proportional to $1/v$ and thus increases with decreasing velocity v . But it is also found that the *firing rate* λ *decreases* with fatigue, perhaps due to adaptation. The firing rate affects the factor (7) since the number of pulse n is given by $n = \lambda t$ where t is the time of measurement. Thus, averaging over the time t we get the factor λ and we would therefore predict the *energy* to change as λ/v .

The combined observed effect is that the energy tends to *increase* with fatigue for sEMG, but to *decrease* for EMG measured with indwelling electrodes. The explanation may be that in the case of the sEMG the shift of the spectrum toward the lower end means that a larger part of the energy will reside inside its bandpass interval, determined by the skin and tissue and the distance between the electrodes, enough to offset the decrease due to the lowered firing rate (see [Basmaijan & de Luca, 1985] p. 92 – 94, and ch. 8 on muscle fatigue). For indwelling electrodes the bandwidth is much larger and there is no similar effect of a "shadowed energy coming into light".

It is common to measure sEMG using *bipolar electrodes*; that is, with two detecting surfaces. Suppose the electrodes are aligned along the axis of the muscle fibres with a separation d . The potential difference between the electrodes due to a travelling wave (1) would be

$$(15) \quad h(t) = g(x+d-vt) - g(x-vt)$$

whose Fourier transform is

$$(16) \quad \hat{h}(f) = e^{-i2\pi f \frac{x}{v}} \cdot \left(1 - e^{-i2\pi f \frac{d}{v}}\right) \cdot \hat{g}\left(\frac{-f}{v}\right)$$

Taking the squared magnitude of (16) we obtain

$$(17) \quad |\hat{h}(f)|^2 = \left\{ 2 \sin\left(\frac{\pi f d}{v}\right) \right\}^2 \cdot \left| \frac{1}{v} \cdot \hat{g}\left(\frac{f}{v}\right) \right|^2$$

Thus, the spectrum is modulated by a geometrical sinus-factor with *pass frequencies* given by

$$(18) \quad f = \left(n + \frac{1}{2} \right) \cdot \frac{v}{d}$$

and the *cancellation frequencies* given by

$$(19) \quad f = n \cdot \frac{v}{d}$$

for $n = 1, 2, 3, \dots$ For bipolar surface electrodes we may have $d = 0.01$ m, which for $v = 4$ m/s gives a cancellation frequency ($n = 1$) of 400 Hz. For needle electrodes we may have a separation around $d = 5 \cdot 10^{-4}$ m which gives a corresponding cancellation frequency of 8000 Hz. In careful measurements the dip in the spectrum around the cancellation frequency v/d can be observed and used for determining the conduction velocity v .

An interesting observation is that there seems to be a kind of a natural background oscillations of the muscles at constant-force contractions.

"The fluctuations in force which are ever present during attempted constant-force contractions are a manifestation of low frequency oscillations which are inherent in the firing rates of the motor units. The dominant frequency of this oscillation is approximately 1.5 Hz. The source of this oscillation has not been identified yet" [Basmajian & de Luca, p. 152].

Basmajian & de Luca notes later that this phenomenon may perhaps be related to another property of the muscle. If the muscle is exercised with a sinusoidal varying force at isometric conditions one may estimate the transfer function of the mechano-electric system between the integrated rectified EMG and the force. One quoted approximate result for the transfer function is (from [Basmajian & de Luca, 1985, p. 197] which refers to results by Soechting and Roberts, 1975)

$$(20) \quad \frac{1}{(i2\pi f + 5\pi)^2}$$

which thus acts as low pass filter with the cutoff frequency of 2.5 Hz which is of the same order as the frequency of the "natural oscillation" of the muscle.

2.2.2.1 Model of IAP

A popular mathematical model for the *intracellular action potential* (IAP) is given as a function of space co-ordinate by (see e.g. [Stegeman et al., 2000])

$$(1) \quad IAP(x) = Ax^3 e^{-\lambda x} \cdot \Theta(x) - B$$

with parameters A , B and λ which can be chosen so that (1) fits the observed potentials. (The Heviside function $\Theta(x)$ on the RHS makes the first term zero for $x < 0$.) From the action potential (1) we may also derive the corresponding transmembrane current I_m . Indeed, the classical *cable equation*

$$(2) \quad I_m = C_m \frac{\partial \phi}{\partial t} + I_{lon} = \frac{\sigma a}{2} \cdot \frac{\partial^2 \phi}{\partial x^2}$$

(see e.g. [Keener & Sneyd, 1998, ch. 8] for an intensive treatment, and for a more extensive treatment, see [Koch, 1999], a book which is largely devoted to the applications of the cable equation to physiology) goes back to works by Lord Kelvin (1859) and Oliver Heaviside (1876) on the theory of the transatlantic cable and was imported into physiology foremost by Hodgkin and Rushton (1946). Though Eq (2) is a relatively simple consequence of the basic "laws" of Ohm and Kirchoff in the theory of electricity it has profound consequences.

In the present context ϕ in Eq (2) is the potential difference across the membrane, C_m is the capacitance per unit area of the membrane, I_m is the total transmembrane current density, I_{lon} is the ohmic part of the transmembrane current density, σ is the electrical conductivity along the fibre axis, and a is the radius of the fibre. Identifying I_m with IAP above we obtain that I_m is proportional to the second derivative of the IAP potential,

$$(3) \quad I_m(x) = \frac{\sigma a}{2} \cdot \frac{d^2 IAP(x)}{dx^2}$$

where a is the radius of the fibre and σ is the electrical conductivity along the fibre axis (which here coincides with the x -axis). Since the extracellular space generally have quite high conductivity the potential is nearly *constant on the outer side* of the membrane. It is therefore the current density (3) which carries the information about the potential changes *in the cell* to the outside world. This is described in the next section on the volume conductor model.

The cable equation (2) allows for pulse-like waves (action potentials) in the fibre as was shown in the pioneering works by Hodgkin, Huxely and Katz (1954). By taking into account the active ion pumps of the cell, the I_{lon} will be described as a nonlinear function of the potential. This in turn is the mathematical basis for the existence of the pulse-like solutions. It may be fitting here to quote the words by Keener and Sneyd (p. 121) on the

Hodgkin-Huxley-Katz contribution: "In biology, where quantitatively predictive theories are rare, this work stands out as one of the most successful combinations of experiment and theory". However, some of the basic tenets of the ion pump theory have been challenged by G Ling [Ling 2001] and G H Pollack [Pollack 2001] on both experimental and theoretical grounds.

2.2.2.2 The volume conductor model

Consider first the simple case of a homogenic resistive medium with the current density \mathbf{J} and the potential ϕ related by the ohmic relation

$$(1) \quad -\sigma \nabla \phi = \mathbf{J}$$

where σ is the conductivity (Eq (1) is essentially a continuum rendering of "Ohm's law" $U = RI$). Taking the divergence of Eq (1) and assuming σ to be constant we obtain

$$(2) \quad -\sigma \nabla^2 \phi = \nabla \cdot \mathbf{J} = I_s$$

The last equality in Eq (2) defines the *current source* I_s . In order to elucidate the meaning of the current source term we integrate it over a volume V bounded by a surface S using Gauss' divergence theorem

$$(3) \quad \int_V \nabla \cdot \mathbf{J} dV = \int_S \mathbf{J} \cdot d\mathbf{S}$$

Suppose S is the surface bounding a muscle fibre, then the RHS of Eq (3) gives the current flowing through the surface (the transmembrane current). Comparing Eqs (2) of this and the previous sections we infer that for a cylindrical fiber of radius a we have

$$I_s = \frac{2}{a} I_m$$

Muscle fibers are however not electrically isotropic. The conductivity along the axis of the fibre is about five times the radial conductivity. Typical values are given in the table below (quoted from [Roeleveld et al., 1997])

| Conductivity σ (1/Ohm·m) | Tissue |
|---------------------------------|-------------------------------|
| 0,10 | Muscle, radial (σ_r) |
| 0,50 | Muscle, axial (σ_x) |
| 0,05 | Fat (isotropic) |
| 1,00 | Skin (isotropic) |

The Eq (2) is simple to adapt to the case of the anisotropic muscle. In terms of cylindrical co-ordinates the Poisson equation becomes (the fiber axis along the z -axis)

$$(4) \quad \sigma_r \left(\frac{1}{r^2} \frac{\partial^2 \phi}{\partial \varphi^2} + \frac{1}{r} \frac{\partial}{\partial r} \left(r \frac{\partial \phi}{\partial r} \right) \right) + \sigma_z \frac{\partial^2 \phi}{\partial z^2} = -I_m$$

In one of the oldest models, described e.g. in [Stegeman et al., 2000], one considers the case of a fibre in the muscle. The muscle tissue is assumed to be a volume conductor of infinite extent bounded by an infinite plane Γ , representing the skin, which is taken to be parallel with the fibre axis. The *boundary condition* for (4) is then that no current passes through the skin,

$$(5) \quad \sigma_r \mathbf{n} \cdot \nabla \phi = 0$$

at the plane Γ

where \mathbf{n} denotes the normal of the plane. Suppose that the plane Γ is at a distance $d/2$ from the fibre. Now it is easy to construct a solution for (4 - 5) from the solutions ϕ_0 in the case of an unrestricted infinite volume conductor using the mirroring method. Indeed, if we add two such solutions, one with the fibre on the right side of the plane, the other with the fiber on the mirror side of the plane,

$$(6) \quad \phi(\mathbf{r}) = \phi_0(\mathbf{r}) + \phi_0(\mathbf{r} - \mathbf{d})$$

then it can be shown that it satisfies the boundary condition (5). Especially on the skin (the plane Γ) we obtain

$$(7) \quad \phi(\mathbf{r}) = 2\phi_0(\mathbf{r})$$

for $\mathbf{r} \in \Gamma$

These results are based on the fact that in the isotropic case ϕ_0 is a simple sum or integral of $1/|\mathbf{r}|$ -potentials (which all satisfy Eq (2) in the region where $I_s = 0$). The solution in anisotropic case can be obtained from the isotropic solution by rescaling the z -variable as

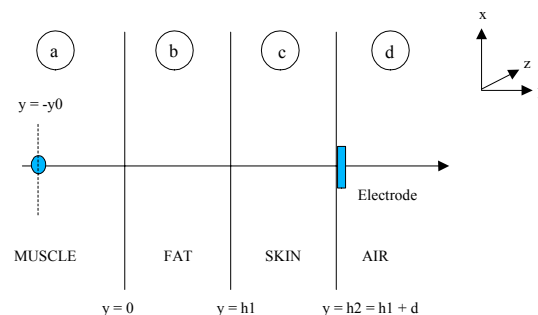
$\sqrt{\frac{\sigma_r}{\sigma_z}} \cdot z$. This leads finally to the expression

$$(8) \quad \phi(r, z) = \frac{2}{4\pi\sigma_r} \int_0^L \frac{2\pi a I_m(s)}{\sqrt{r^2 \frac{\sigma_r}{\sigma_z} + (z-s)^2}} ds$$

for the potential at the skin due to a MAP in a fibre of length L and radius a . The next step is to add more realistic details to the model by considering the fatty tissue and the properties of the skin.

2.2.2.3 A four-layer model

We will describe a simple four-layer model [Farina & Rainoldi, 1999] which gives an idea how the tissue affects the current generated signal in the muscle. In this model we have a sandwich consisting of a muscle layer (a), a fat layer (b), and finally a skin layer (c) which interfaces with the air (d). The y-axis is taken to be orthogonal to the sections, the x-axis is along the plane orthogonal to the direction of the muscle, whereas the z-axis is taken to be along the muscle.



All the layers are supposed to be isotropic except for the muscle layer which has different conductivities in the transversal (x-axis) and the axial directions (z-axis) as pointed out in the previous section. The current source is supposed to be a unit point source located at $(0, -y_0, 0)$

$$(1) \quad I_m(x, y, z) = \delta(x) \delta(y + y_0) \delta(z)$$

The solution for a general current source can then be obtained by summing solutions for point sources. This is an example of the methods of the *Green's function* in mathematical physics [Wallace, 1984]. If we have some linear differential equation

$$(2) \quad \Lambda \phi(\mathbf{r}) = \rho(\mathbf{r})$$

then a Green's function $G(\mathbf{r})$ is a solution of the point source equation

$$(3) \quad \Delta G(\mathbf{r}) = \delta(\mathbf{r})$$

and the solution to (2) can then be obtained from

$$(4) \quad \phi(\mathbf{r}) = \int G(\mathbf{r}-\mathbf{s}) \rho(\mathbf{s}) d\mathbf{s}$$

In signal processing the *transfer function* – the response H to a delta-signal input – is the counterpart of the Green's function. Following [Farina & Rainoldi, 1999] we will study the solution of (2) in term of the Fourier transformed field

$$(5) \quad \tilde{\phi}(k_x, y, k_z) = \int \int e^{-ik_x x - ik_z z} \phi(x, y, z) dx dz$$

The Eq (4) of the previous section then becomes in the present problem, with the unit current source (1), the following set of equations ($\sigma_{ax} = \sigma_{ay} \neq \sigma_{az}$):

$$(6) \quad \begin{aligned} (\partial_y^2 - k_{ay}^2) \tilde{\phi}(y) &= \frac{1}{\sigma_{ay}} \delta(y + y_0) \\ k_{ay} &= \sqrt{k_x^2 + \frac{\sigma_{az}}{\sigma_{ay}} k_z^2} \end{aligned}$$

for layer (a), and for the other layers ($\sigma_x = \sigma_y = \sigma_z$) we get similar equations

$$(7) \quad \begin{aligned} (\partial_y^2 - k_y^2) \tilde{\phi}(y) &= 0 \\ k_y &= \sqrt{k_x^2 + k_z^2} \end{aligned}$$

whose solutions are composed of simple exponential functions $e^{\pm ky}$ while in the layer (a) we have an "inhomogenic" solution of the type $e^{-k|y + y_0|}$ plus the homogenic ones $e^{\pm ky}$. The boundary conditions are that the field, and the current density \mathbf{J} (Eq (1) in the previous section), should be continuous at the layer interfaces,

$$(8) \quad \begin{aligned} (\sigma \nabla \phi)_- &= (\sigma \nabla \phi)_+ \\ (\phi)_- &= (\phi)_+ \end{aligned}$$

where "-" ("+") means the left (right) side limit value at a layer interface. Together with the requirement that $\phi(y)$ goes to zero as $y \rightarrow \pm\infty$, these equations and conditions determine a unique solution. In fact, we have already used (8) in Eqs (6) and (7) for the x and z directions when using the fact that k_x and k_z do not change going from one layer to another for solutions having an x - and a z -dependence of the form $e^{k_x x + k_z z}$. The general solution for each layer can be written

$$(9) \quad \tilde{\phi}_a = \frac{1}{2k_{ay}} e^{-k_{ay}|y+y_0|} + u_a e^{k_{ay}y} \quad (y < 0)$$

$$\tilde{\phi}_b = u_b e^{k_y y} + v_b e^{-k_y y}$$

$$\tilde{\phi}_c = u_c e^{k_y y} + v_c e^{-k_y y}$$

$$\tilde{\phi}_d = v_d e^{-k_y y} \quad (y > h_1 + d)$$

with the u - and v -parameters to be determined by the boundary conditions (8). These conditions result in a matrix equation

$$(10) \quad K \begin{pmatrix} \frac{1}{k_{ay}} e^{-k_{ay}y_0} + u_a \\ -\frac{\sigma_{ay}}{2} e^{-k_{ay}y_0} + u_a k_{ay} \sigma_{ay} \end{pmatrix} = \begin{pmatrix} v_d e^{-k_y(h_1+d)} \\ 0 \end{pmatrix}$$

where the matrix K is given by

$$(11) \quad K = \frac{1}{\sigma_{by} \sigma_{cy} k^2} \begin{pmatrix} k^2 D & k B \\ k^3 C & k^2 A \end{pmatrix}$$

The functions A , B , C and D are in turn given by

$$(12) \quad \begin{aligned} A &= \sigma_{cy} (\sigma_{by} \cosh(k_y h_1) \cosh(k_y d) + \sigma_{cy} \sinh(k_y h_1) \sinh(k_y d)) \\ B &= \sigma_{by} \cosh(k_y h_1) \sinh(k_y d) + \sigma_{cy} \sinh(k_y h_1) \cosh(k_y d) \\ C &= \sigma_{by} \sigma_{cy} (\sigma_{by} \sinh(k_y h_1) \cosh(k_y d) + \sigma_{cy} \cosh(k_y h_1) \sinh(k_y d)) \\ D &= \sigma_{by} (\sigma_{by} \sinh(k_y h_1) \sinh(k_y d) + \sigma_{cy} \cosh(k_y h_1) \cosh(k_y d)) \end{aligned}$$

Thus, from Eq (10) we can solve for u_a ,

$$(13) \quad u_a = \frac{e^{-k_{ay}y_0}}{2k_{ay}} \cdot \left(\frac{Ak_{ay}\sigma_{ay} - Ck_y}{Ak_{ay}\sigma_{ay} + Ck_y} \right)$$

Finally, we can solve for v_d in term of u_a ,

$$(14) \quad \frac{e^{-k_{ay}y_0}}{2} \left(\frac{k_y D}{k_{ay}} - B\sigma_{ay} \right) + u_a \cdot (k_y D + k_{ay}\sigma_{ay} B) \\ = v_d \cdot (\sigma_{by}\sigma_{cy}k_y e^{-k_y(h_1+d)})$$

that is,

$$(15) \quad \frac{e^{-k_{ay}y_0}}{2k_{ay}} \left\{ \left(\frac{k_y D - k_{ay}\sigma_{ay} B}{k_y D + k_{ay}\sigma_{ay} B} \right) + \left(\frac{Ak_{ay}\sigma_{ay} - Ck_y}{Ak_{ay}\sigma_{ay} + Ck_y} \right) \right\} \\ = v_d \cdot \left(\frac{\sigma_{by}\sigma_{cy}k_y e^{-k_y(h_1+d)}}{k_y D + k_{ay}\sigma_{ay} B} \right)$$

which, using

$$AD - BC = \sigma_{by}^2 \sigma_{cy}^2$$

can finally be simplified to

$$(16) \quad v_d e^{-k_y(h_1+d)} = e^{-k_{ay}y_0} \frac{\sigma_{ay}\sigma_{by}\sigma_{cy}}{Ak_{ay}\sigma_{ay} + Ck_y}$$

As pointed out by [Farina & Rainoldi, 1999] one can use this theoretical model to invert the filtering of the tissue and thus even resolve individual MUAPs from the sEMG data. These aspects will be developed further in the second part.

Bibliography

(The "LANL-archive" can be accessed at xxx.lanl.gov)

1. Abarbanel H D I: *Analysis of Observed Chaotic Data*. Springer 1995.
2. Abramowitz M, Stegun I A: *Handbook of Mathematical Functions*. Dover 1965.
3. Akay M (Ed.): *Nonlinear Biomedical Signal Processing*. Volume II. Dynamic Analysis and Modeling. IEEE Press 2001.
4. Akay M (Ed.): *Time Frequency and Wavelets in Biomedical Signal Processing*. IEEE Press 1998.
5. Alligood K T, Sauer T D, Yorke J A: *Chaos. An Introduction to Dynamical Systems*. Springer 1996.
6. Askenazy Y et al.: "Discrimination of the healthy and sick cardiac autonomic nervous system by a new wavelet analysis of heartbeat intervals". LANL-archive physics/9804030.
7. Askenazy Y et al.: "Magnitude and sign correlations in heartbeat fluctuations". LANL-archive cond-mat/0005365.
8. Baier G, Leder R S, Parmanada P: "Human electroencephalogram induces transient coherence in excitable spatiotemporal chaos". *Phys. Rev. Lett.* Vol. 84. No. 19 (2000) 4501 - 4504.
9. Bai-Lin H: *Elementary Symbolic Dynamics and Chaos in Dissipative Systems*. World Scientific 1989.
10. Basmajian J V, De Luca C J: *Muscles Alive. Their Functions Revealed by Electromyography*. 5. ed. Williams & Wilkins 1985.
11. Beran J: *Statistics for Long-Memory Processes*. Chapman & Hall/CRC 1994.
12. Bernaola-Galván P et al.: "Scale invariance in the nonstationarity of physiological signals". LANL-archive cond-mat/0005284 v2.
13. Bialek W, Nemenman I, Tishby N: "Complexity through nonextensivity". LANL-archive physics/0103076.
14. Blumenfeld L A, Tikhonov A N: *Biophysical Thermodynamics of Intracellular Processes. Molecular Machines of the Living Cell*. Springer 1994.
15. Bulsara A R, Gammaitoni L: "Tuning in to noise". *Physics Today*. Vol. 49. Issue 3 (March 1996) 39 – 45.
16. Cardy J: *Scaling and Renormalization in Statistical Physics*. Cambridge University Press 1996.
17. Chiari L, Bertani A, Cappello A: "Classification of visual strategies in human postural control". *Human Movement Science* 19 (2000) 817 – 842.
18. Chow C C, Collins JJ: "Pinned polymer model of posture control". *Physical Review* Vol. 52. No. 1 (1995) 907 – 912.
19. Clancy E A: "Probability density of the surface electromyogram and its relation to amplitude detectors". *IEEE Trans. Biomed. Eng.* Vol. 46. No. 4. (1999) 730 – 739.
20. Coch M et al.: "Die fraktale Dimension: Eine nichtlineare Analyseverfahren zur Beschreibung der Herzfrequenzvariabilität". *Herzsch. Elektrophys.* 9 (1998) 212 – 221.
21. Collins J J, De Luca C J: "Random walking during quiet standing". *Phys. Rev. Lett.* Vol. 73. No. 5 (1994) 764 – 767.
22. Cordo P, Harnad S (Eds.): *Movement Control*. Cambridge University Press 1994.

23. Costa M, Goldberger A L, Peng C.-K: "Multiscale entropy analysis of complex physiologic time series". *Phys. Rev. Lett.* 89, 068102(4) (2002).
24. Craigmile P F, Percival D B: "Wavelet-based trend detection and estimation". Preprint 2000.
25. Daoud M, Williams C E (Eds.): *Soft Matter Physics*. Springer 1999.
26. Daune M: *Molecular Biophysics. Structures in Motion*. Oxford University Press 1999.
27. Diks C: *Nonlinear Time Series Analysis*. World Scientific 1999.
28. Dimitrova N, Dimitrov G: "Distance-dependent effects of anatomical and physiological parameters on EMG signals". Proc. of the first general SENIAM workshop. Torino, Italy, September 1996.
29. Ding M, Yang W: "Distribution of the first return time in fractional Brownian motion and its application to the study of on-off intermittency". *Physical Review E* Vol. 52. No. 1 (1995) 207 – 213.
30. Dremine I M, Ivanov O V, Nechitalio V A: "Wavelets and their use". LANL-archive hep-ph/0101182.
31. Duarte M, Zatsiorsky V M: "On fractal properties of natural human standing". *Neuroscience Letters* 283 (2000) 173 – 176.
32. Eckert C, Planat M: "Detection of chaos in the noise of electronic oscillators by time series analysis methods". *Lecture Notes in Physics*. Vol. 550 (2000) 288 – 304. Springer.
33. Eckmann J P, Kamphorst S O, Ruelle D: "Recurrence plots of dynamical systems". *Europhys. Lett.* 4 (1987) 973.
34. Elbert T et al.: "Chaos and physiology: Deterministic chaos in excitable cell assemblies". *Physiological Reviews* Vol. 74, No. 1 (1994) 1 – 47.
35. Engbert R et al.: "Symbolic dynamics of bimanual production of polyrhythms". In [Kantz et al. (Eds.), 1998].
36. Engquist B, Schmid W (Eds.): *Mathematics Unlimited – 2001 and Beyond*. Springer 2001.
37. Farina D, Merletti R: "A novel approach for precise simulation of the EMG signal detected by surface electrodes". *IEEE Trans. Biom. Eng.* 48. No. 6 (2001) 637 – 646.
38. Farina D, Merletti R: "Comparison of algorithms for estimation of EMG variables during voluntary isometric contractions". *J. Electromyogr. Kinesiol.* 10 (2000) 337 – 349.
39. Farina D, Rainoldi A: "Compensation of the effect of sub-cutaneous tissue layers on surface EMG: A simulation study". *Medical Engineering & Physics* 21 (1999) 487 – 496.
40. Filligoi G C, Felici F: "Detection of hidden rhythms in surface EMG signals with nonlinear time-series tools". *Medical Engineering & Physics* 21 (1999) 439 – 448.
41. Finney C E A, Green J B, Daw C S: "Symbolic time-series analysis of engine combustion measurements". *Society of Automotive Engineers*. Paper No. 980624. <<http://citeseer.nj.nec.com/green98symbolic.html>>
42. Flyberg H et al (Eds.): *Physics of Biological Systems. From Molecules to Species*. Springer 1997.
43. Gagey P-M, Weber B: *Posturologie. Régulation et Dérèglements de la Station Debout*. 2. ed. Masson 1999.
44. Gagey P-M, Bizzo G: "Measure in posturology". <<http://perso.club-internet.fr/pmgagey/MeasureEnPosturologie-a.htm>> (Retrieved 15.6.2001.)
45. Gagey P-M: "Should we save the VFY?". <<http://perso.club-internet.fr/pmgagey/VFYSauver-a.htm>> (Retrieved 15.6.2001.)

46. Gammaitoni L et al.: "Stochastic Resonance". *Rev. Mod. Phys.* Vol. 70. No. 1 (1998) 223 – 287.
47. Goychuk I, Hänggi: "Stochastic resonance in ion channels characterized by information theory". LANL-archive cond-math/9919354.
48. Grassberger P, Procaccia I: "Characterization of strange attractors". *Phys. Rev. Lett.* 50 (1983) 346 – 349.
49. Grimnes S, Martinsen Ø S: *Bioimpedance and Bioelectricity Basics*. Academic Press 2000.
50. Haken H: "Nonlinearities in biology: The brain as an example". *Lecture Notes in Physics*. Vol 542 (2000) 427 – 445. Springer.
51. Haken H: *Advanced Synergetics*. Springer 1983.
52. Hänsler E: *Statistische Signale*. 2. Aufl. Springer 1997.
53. Harris J W, Stocker H: *Handbook of Mathematical and Computational Science*. Springer 1998.
54. Hastings H, Sugihara G: *Fractals – A User's Guide for The Natural Sciences*. Oxford University Press 1993.
55. Haykin S: *Neural Networks – A Comprehensive Foundation*. 2. ed. Prentice Hall 1999.
56. Hegger R, Kantz H, Matassini L: "Denoising human speech signals using chaotic features". *Phys. Rev. Lett.* Vol. 84. No. 14 (2000) 3197 - 3200.
57. Hegger R, Kantz H, Olbrich E: "Problems in the reconstruction of high-dimensional deterministic dynamics from time series". In [Kantz et al. (Eds.), 1998].
58. Hegger R, Kantz H, Schreiber T: "Practical implementation of nonlinear time series methods. The TISEAN package." LANL-archive chao-dyn/9810005.
59. Henry B, Lovell N, Camacho F: "Nonlinear dynamics time series analysis". In [Akay (Ed.), 2001].
60. Hentschel H G E, Procaccia I: "The infinite number of generalized dimensions of fractals and strange attractors". *Physica D* 8 (1983) 435 - 444.
61. Hoppensteadt F C, Peskin C S: *Modeling and Simulation in Medicine and the Life Sciences*. 2 ed Springer 2002.
62. Hugdahl K: *Psychophysiology. The Mind-Body Perspective*. Harvard University Press 1995.
63. Hulata E et al.: "Detection and sorting of neural spikes using wavelet packets". *Phys. Rev. Lett.* Vol. 85. No. 21 (2000) 4637 - 4640.
64. Hwa R C, Ferree T C: "Fluctuation analysis of human electroencephalogram". LANL-archive arXiv: physics/0104029 (10 May 2001).
65. Hyvärinen A, Oja E: "Independent component analysis: A tutorial" (April 1999). Laboratory of Computer and Information Science, Helsinki University of Technology. <www.cis.hut.fi/projects/ica>
66. Iasemidis L D, Principe J C, Sackellares J S: "Measurement and quantification of spatio-temporal dynamics of human epileptic seizures". (In *Nonlinear Signal Processing in Medicine*. Ed. M Akay. IEEE Press 1999.) Online version at <www.citeseer.nj.nec.com/iasemidis99measurement.html>.
67. Jeong B Y: "Contour representation of sway area in posturography and its application". *Arch. Phys. Med. Rehabil.* 75 (1994) 951 – 955.
68. Jeong J, Joung M K, Kim S Y: "Quantification of emotion by nonlinear analysis of the chaotic dynamics of electroencephalograms during preception of 1/f music". *Biological Cybernetics* 78 (1998) 217 – 225.
69. Jones C K R T: "Whither applied nonlinear dynamics?" In [Engquist & Schmid (Eds.), 2001].

70. José J V, Saletan E J: *Classical Dynamics. A Contemporary Approach*. Cambridge University Press 1998.
71. Jülicher F: "Mechanical oscillations at the cellular scale". LANL-archive physics/0106071 v1 (21 Jun 2001).
72. Kantz H, Kurths H, Mayer-Kress G (Eds.): *Nonlinear Analysis of Physiological Data*. Springer 1998.
73. Kantz H, Schreiber T: *Nonlinear Time Series Analysis*. Cambridge University Press 1997, 2000.
74. Karamanos K: "From symbolic dynamics to digital approach: Chaos and transcendence". *Lecture Notes in Physics*. Vol. 550 (2000) 357 – 371. Springer.
75. Keener J, Sneyd J: *Mathematical Physiology*. Springer 1998.
76. Kennel M B, Isabelle S: "Method to distinguish chaos from colored noise and to determine embedding parameters". *Phys. Rev. A* (1992) 3111 - 3118.
77. Khoo M C K: *Physiological Control Systems: Analysis, Simulation, and Estimation*. IEEE Press 2000.
78. Koch C: *Biophysics of Computation*. Oxford University Press 1999.
79. Kopell N: "We got rhythm: Dynamical systems of the nervous system". *Notices of the AMS*. Vol. 47. No. 1. 2000. <www.ams.org/notices>
80. Landsberg P T: *Thermodynamics and Statistical Mechanics*. Dover 1990.
81. Lauk M et al.: "Assessing muscle stiffness from quiet stance in Parkinson's disease". *Muscle & Nerve* 22 (1999) 635 – 639.
82. Lauk M et al.: "Human balance out of equilibrium: Nonequilibrium statistical mechanics in posture control". *Phys. Rev. Lett.* Vol. 80. No. 2 (1998) 413 – 416.
83. Liebovitch L S, Yang W: "Transition from persistent to antipersistent correlation in biological systems". *Physical Review E* Vol. 56 No. 4 (1997) 4557 – 4566.
84. Ling G: *A Revolution in the Physiology of the Living Cell*. Pacific Press 2001.
85. Lorenz E N: "Deterministic nonperiodic flow". *Journal of Atmospheric Sciences* 20 (1963) 130 - 141.
86. Mackey M C, Glass G L: "Oscillation and chaos in physiological systems". *Science* 197 (1977) 287 – 289.
87. Mäkikallio T: *Analysis of Heart Rate Dynamics by Methods Derived From Nonlinear Mathematics*. University of Oulu 1998. (Ph.D. thesis.)
88. Mäkikallio T et al.: "Abnormalities in beat to beat complexity of heart rate dynamics in patients with previous myocardial infarction". *J. Am. Coll. Cardiol.* 28 (1996) 1005 - 1011.
89. Malmivuo J, Plonsey R: *Bioelectromagnetism. Principles and Applications of Bioelectric and Biomagnetic Fields*. Oxford University Press 1995.
90. Mandelbrot B: *Multifractals and 1/f-noise*. Springer 1999.
91. Mandelbrot B: *The Fractal Geometry of Nature*. Freeman 1982.
92. Marek M, Schreiber I: *Chaotic Behaviour of Deterministic Dissipative Systems*. Cambridge University Press 1991.
93. Mazumdar J: *An Introduction to Mathematical Physiology & Biology*. 2. ed. Cambridge University Press 1999.
94. McCauley J L: *Chaos, Dynamics and Fractals. An Algorithmic Approach to Deterministic Chaos*. Cambridge University Press 1994.
95. Mees A I (Ed.): *Nonlinear Dynamics and Statistics*. Birkhäuser 2001.
96. Melkonian D, Blumenthal T, Gordon E: "Numerical Fourier transform spectroscopy of EMG half-wave: Fragmentary-decomposition-based approach to nonstationary signal analysis". *Biological Cybernetics* 81 (1999) 457 – 467.
97. Milton J G: "Epilepsy – Multistability in a dynamic disease". In [Walczek, 2000].

98. Mischaikov et al.: "Construction of symbolic dynamics from experimental time series". Preprint 1998.
99. Moschytz G, Hofbauer M: *Adaptive Filter*. Springer 2000.
100. Moss F: "Stochastic resonance – looking forward". In [Walczek, 2000].
101. Nieminen H, Takala E-P: "Evidence of deterministic chaos in the myoelectric signal". *Electromyogr. Clin. Neurophysiol.* 36 (1996) 49 – 58.
102. Nigg B M, Herzog W: *Biomechanics of the Musculo-skeletal System*. Wiley 1995.
103. Ösbay H: *Introduction to Feedback Control Theory*. CRC Press 2000.
104. Ott E, Grebogi C, Yorke J A: "Controlling chaos". *Phys. Rev. Lett.* 64 (1990) 1196.
105. Packard N H et al.: "Geometry from a time series". *Phys. Rev. Lett.* 45 (1980) 712 – 716.
106. Palus M: "Nonlinearity in normal human EEG: cycles, temporal asymmetry, nonstationarity and randomness, not chaos". *Biological Cybernetics* 75 (1996) 389 – 396.
107. Papoulis A: *Probability, Random Variables, and Stochastic Processes*. McGraw-Hill 1991.
108. Peng C-K, Hausdorff J M, Goldberger A L: "Fractal mechanism in neuronal control: Heartbeat and gait dynamics in health and disease". In [Walczek, 2000]. Online: <<http://reylab.bidmc.harvard.edu/tutorial/DFA/master.html>>.
109. Peng C-K et al.: "Mosaic organization of DNA nucleotides". *Physical Review E*. Vol. 49 No. 2 (1994) 1685 – 1689.
110. Peterka R J: "Postural control model interpretation of stabilogram diffusion analysis". *Biological Cybernetics* 82 (2000) 335 – 343.
111. Peterson I: *Newton's Clock - Chaos in the Solar System*. W H Freeman 1995.
112. Peters T M, Williams J (Eds.): *The Fourier Transform in Biomedical Engineering*. Birkhäuser 1998.
113. Pincus S M: "Approximate entropy as a measure of system complexity". *Proc. Natl. Acad. Sci. USA* 88 (1991) 2297 – 2301.
114. Pincus S M, Goldberger A L: "Physiological time-series analysis: what does regularity quantify?". *Am. J. Physiol. Heart Circ. Physiol.* 266: H1643 – H1656 (1994).
115. Pokorný J, Wu T-M: *Biophysical Aspects of Coherence and Biological Order*. Springer 1998.
116. Pollack G H: *Cells, Gels and The Engines of Life. A New Unifying Approach to Cell Functions*. Ebner & Sons 2001.
117. Prigogine I, Stengers I: *Order Out of Chaos*. Heinemann 1984.
118. Quarteroni A: "Modelling the cardiovascular system: A mathematical challenge". In [Engquist & Schmid (Eds.), 2001].
119. Quarteroni A: *Modellistica Numerica per Problemi Differenziali*. Springer 2000.
120. Råde L, Westergren B: *Mathematics Handbook for Science and Engineering*. Studentlitteratur 1998.
121. Rangarajan G, Dings M: "An integrated approach to the assessment of long range correlation in time series data". LANL-archive cond-mat/0105269 v1 (14 May 2001).
122. Rangayyan R M: *Biomedical Signal Analysis. A Case-Study Approach*. IEEE Press 2002.
123. Rangayyan R M et al.: "Parametric representation and screening of knee joint vibroarthrographic signals". *IEEE Transactions on Biomedical Engineering*. Vol 44. No. 11 (1997) 1068 – 1074.

124. Rao V B, Rao H V: *Neural Networks and Fuzzy Logic*. 2. ed. MIS Press 1995.
125. Rapp P E, Schmach T I, Mess A I: "Models of knowing and the investigation of dynamical systems". *Physica D* 132 (1999) 133 – 149.
126. Reguera D et al.: *Statistical Mechanics of Biocomplexity*. (Proceedings. Sitges, Barcelona, Spain 1998). Springer 1999.
127. Ricciardi L M: *Diffusion Processes and Related Topics in Biology*. (Lecture Notes in Biomathematics 14.) Springer 1977.
128. Richman J S, Moorman J R: "Physiological time-series analysis using approximate entropy and sample entropy". *Am. J. Physiol. Heart Circ. Physiol.* 278: H2039 – H2049 (2000).
129. Richter M, Schreiber T: "Phase space embedding of electrocardiograms". LANL-archive chao-dyn/9807035.
130. Rieke F, Warland D, Steveninck R de R van, Bialek W: *Spikes. Exploring the Neural Code*. MIT Press 1999, 1997.
131. Roeleveld K et al.: "Volume conduction models for surface EMG; confrontation with measurements". *J. Electromyogr. Kinesiol.* Vol 7. No. 4. (1997) 221 - 232.
132. Rosenblum M et al.: "Human postural control: Force plate experiments and modelling". In [Kantz et al. (Eds.), 1998].
133. Rougier P: "Influence of visual feedback on successive control mechanisms in upright quiet stance in humans assessed by fractional Brownian motion modelling". *Neuroscience Letters* 266 (1999) 157 – 160.
134. Ruelle D: *Chaotic Evolution and Strange Attractors*. Cambridge University Press 1989.
135. Ruelle D: "Where can one hope to profitably apply the ideas of chaos?". *Physics Today*. Vol. 47. Issue 7 (4 July 1994) 24 - 30.
136. Sackellares J S et al.: "Epilepsy when chaos fails". (In *Chaos in the Brain?* Eds. K Lehnertz, C E Elgar. World Scientific.) Online version at www.citeseer.nj.nec.com/282786.html.
137. Saichev A I, Woyczyński W A: *Distributions in the Physical and Engineering Sciences*. Vol. 1. Birkhäuser 1997.
138. Sakuranga M et al.: "Nonlinear analysis: Mathematical theory and biological applications". *CRC Critical Reviews in Biomedical Engineering*. Vol 12. Issue 2 (1986) 127 – 184.
139. Schneidman E et al.: "Universality and individuality in neural code". LANL-archive physics/0005043.
140. Schreiber T, Kaplan D T: "Signal separation by nonlinear projections: the fetal electrocardiogram". *Phys. Rev. E* 53 (1996) 4326.
141. Schreiber T, Schmitz A: "Surrogate time series". LANL-archive chao-dyn/9909037 (27 Sep 1999).
142. Schreiber T: "Interdisciplinary applications of nonlinear time series methods". Habilitationsschrift, Wuppertal. LANL-archive chao-dyn/9807001; *Physics Reports* 308, 1 (1998)
143. Schreiber T: "Nonlinear time series analysis: Measuring information transport". Preprint 2000.
144. Schreiber T: "Processing of physiological data". In [Kantz et al. (Eds.), 1998].
145. Schroeder M: *Fractals, Chaos, Power Laws. Minutes From the Infinite Paradise*. W H Freeman 1991.
146. Schulte-Frohlinde V et al.: "Noise effects on the complex patterns of abnormal heartbeats". LANL-archive cond-mat/0011367.
147. Shannon C E, Weaver W: *The Mathematical Theory of Information*. University of Illinois Press 1949.

148. Signorini M G, Sassi R, Cerutti S: "Assessment of nonlinear dynamics in heart rate variability signal". In [Akay (Ed.), 2001].
149. Simmons G F: *Differential Equations. With Applications and Historical Notes*. McGraw-Hill 1972.
150. Sinha S, Pande A, Pandit R: "Defibrillation via the elimination of spiral turbulence in a model for ventricular fibrillation". *Phys. Rev. Lett.* Vol. 86. No. 16 (2001) 3678 - 3681.
151. Skinner J E, Zebrowski J J, Zbigniew J K: "New nonlinear algorithms for analysis of heart rate variability: Low-dimensional chaos predicts lethal arrhythmia". In [Kantz et al. (Eds.), 1998].
152. Sostaric A, Zasula D, Strelec M: "EMG analysis using wavelet transform". Preprint 1995.
153. Stegeman D F et al.: "Surface EMG models: properties and applications". *J. Electromyogr. Kinesiol.* 10 (2000) 313 – 326.
154. Thamilmaran K, Lakshmanan M, Murali K: "Rich variety of bifurcations and chaos in a variant of Murali-Lakshmanan-Chua circuit". LANL-archive nlin.CD/0012056.
155. Thomas D D, dos Remedios C G (Eds.): *Molecular Interactions of Actin. Actin-Myosin Interaction and Actin-Based Regulation*. Springer 2002.
156. Tong H: "A personal overview of non-linear time series analysis from a chaos perspective". *Scand. J. Statist.* 22 (1995) 399 - 445.
157. Tong H: *Non-linear Time Series Analysis*. Oxford University Press 1990.
158. Unser M, Aldroubi A: "A review of wavelets in biomedical applications". *Proc. of the IEEE*. Vol. 84. No 4 (1996) 626 – 638.
159. van der Kooij H et al.: "An adaptive model of sensory integration in dynamic environment applied to human stance control". *Biological Cybernetics* 84 (2001) 103 – 115.
160. Vicsek T (Ed): *Fluctuations and Scaling in Biology*. Oxford University Press 2001.
161. Vidakovic B: *Statistical Modeling by Wavelets*. John Wiley & Sons 1999.
162. Vikman S et al.: "Altered complexity and correlation properties of R-R interval dynamics before spontaneous onset of paroxysmal atrial fibrillation". *Circulation*. 16 November 1999, 2079 - 2085. <www.circulationaha.org>.
163. Wallace Ph R: *Mathematical Analysis of Physical Problems*. Dover 1984.
164. Walleczek J (Ed.): *Self-Organized Biological Dynamics and Nonlinear Control*. Cambridge University Press 2000.
165. Weiss T F: *Cellular Biophysics* (2 Vols). MIT Press 1996.
166. Wellig P, Moschytz, Läubli T: "Decomposition of emg signals using time-frequency features". *Proc. 20th annual Int. Conf. of the IEEE Engineering in Medicine and Biology Society*. Hong Kong 1998.
167. Winter D A et al.: "Ankle muscle stiffness in the control of balance during quiet standing". *J. Neurophysiol.* 85 (2001) 2630 – 2633
168. Winter D A et al.: "Stiffness control of balance in quiet standing". *J. Neurophysiol.* 80 (1998) 1211 – 1221.
169. Yang F, Hong B, Tang Q: "Approximate entropy and its application to biosignal analysis". In [Akay M (Ed.), 2001].
170. Yang W et al.: "Preserving chaos: control strategies to preserv complex dynamics with potential relevance to biological disorders". *Physical Review E* Vol 51. No. 1 (1995) 102 – 110.
171. Yao W, YU P, Essex C: "Delayed stochastic differential model for quiet standing". *Phys. Rev. E* Vol. 63. No. 2 (2001), online version 021902.

172. Zbigniew J K: "Relativity of dynamical measures in study of human brain". In [Kantz et al. (Eds.), 1998].
173. Zbilut J P, Giuliani A, Webber C L: "Recurrence quantification analysis and principal components in the detection of short complex signals". LANL-archive chao-dyn/9712017. (*Phys. Lett. A* 237 (1998) 131.)
174. Zhang Y T et al.: "Adaptive cancellation of muscle contraction interference in vibroarthographic signals". *IEEE Transactions on Biomedical Engineering*. Vol 41. No. 2 (1994) 181 – 191.
175. Zhang Y T et al.: "Mathematical modeling and spectrum analysis of the physiological patello-femorale pulse train produced by slow knee movement". *IEEE Transactions on Biomedical Engineering*. Vol 39. No. 9 (1992) 971 – 979.